JHEP

Published for SISSA by Springer

Received: October 29, 2018
Revised: March 7, 2019
Accepted: March 27, 2019
Published: April 17, 2019

Semi-analytical calculation of gluon fragmentation into $^1S_0^{[1,8]}$ quarkonia at next-to-leading order

Peng Zhang,[a,b] **Chen-Yu Wang,**[a] **Xiao Liu,**[a] **Yan-Qing Ma,**[a,b,c] **Ce Meng**[a] **and Kuang-Ta Chao**[a,b,c]

[a] *School of Physics and State Key Laboratory of Nuclear Physics and Technology, Peking University, Beijing 100871, China*
[b] *Center for High Energy Physics, Peking University, Beijing 100871, China*
[c] *Collaborative Innovation Center of Quantum Matter, Beijing 100871, China*

E-mail: p.zhang@pku.edu.cn, wangcy@pku.edu.cn, xiao6@pku.edu.cn, yqma@pku.edu.cn, mengce75@pku.edu.cn, ktchao@pku.edu.cn

Abstract: We calculate the NLO corrections for the gluon fragmentation functions to a heavy quark-antiquark pair in $^1S_0^{[1]}$ or $^1S_0^{[8]}$ state within NRQCD factorization. We use integration-by-parts reduction to reduce the original expression to simpler master integrals (MIs), and then set up differential equations for these MIs. After calculating the boundary conditions, MIs can be obtained by solving the differential equations numerically. Our results are expressed in terms of asymptotic expansions at singular points of z (light-cone momentum fraction carried by the quark-antiquark pair), which can not only give FFs results with very high precision at any value of z, but also provide fully analytical structure at these singularities. We find that the NLO corrections are significant, with K-factors larger than 2 in most regions. The NLO corrections may have important impact on heavy quarkonia (e.g. η_c and J/ψ) production at the LHC.

Keywords: NLO Computations, QCD Phenomenology

ArXiv ePrint: 1810.07656

https://doi.org/10.1007/JHEP04(2019)116

JHEP04(2019)116

Contents

JHEP04(2019)116

1 Introduction

Study of heavy quarkonium production is important to understand both perturbative and non-perturbative physics in QCD. Currently, the most widely used theory for quarkonium production is the non-relativistic QCD (NRQCD) factorization [1]. Although many important processes have been calculated to next-to-leading order in α_s expansion [2–25], there are still some notable difficulties in quarkonium production within the NRQCD framework (see, e.g. [26]). To further explore the quarkonium production mechanism, it may be better to study quarkonium production at high transverse momentum p_T region, where long-distance interactions between quarkonium and initial-state particles are suppressed and thus factorization is easier to hold.

The inclusive production differential cross section of a specific hadron H at high p_T can be calculated in collinear factorization [27],

$$\mathrm{d}\sigma_{A+B\to H(p_T)+X} = \sum_i \mathrm{d}\hat{\sigma}_{A+B\to i(p_T/z)+X'} \otimes D_{i\to H}(z,\mu) + \mathcal{O}(1/p_T^2)\,, \tag{1.1}$$

where i sums over all quarks and gluons, z is the light-cone momentum fraction carried by H with respect to the parent parton i, and A and B are colliding particles whose effect should be further factorized into partons if they are hadrons. $d\hat{\sigma}_{A+B\to i(p_T/z)+X}$ are perturbatively calculable hard parts, while $D_{i\to H}(z,\mu)$ are non-perturbative but universal fragmentation functions (FFs) describing the probability of parton hadronizing to H with momentum fraction z. For quarkonium production, $\mathcal{O}(1/p_T^2)$ contributions can be further factorized to double parton FFs [28–32]. In both single parton FFs and double parton FFs, there is a collinear factorization scale μ dependence, and this dependence can be canceled between hard parts and FFs perturbatively order by order, leaving physical differential cross section to be independent of the scale. The evolution of single parton FFs with respect to μ are controlled by the Dokshitzer-Gribov-Lipatov-Altarelli-Parisi (DGLAP) evolution equation [33–35], and similar evolution equations for double parton FFs are calculated in [29]. With these evolution equations, the only unknown information for FFs are their values at a chosen factorization scale $\mu = \mu_f$.

When μ_f is close to the quarkonium mass m_H, it is natural to calculate FFs via NRQCD factorization. For single parton FFs that will be considered in this paper, we have

$$D_{i\to H}(z,\mu_f) = \sum_n d_{i\to Q\bar{Q}(n)}(z,\mu_f)\langle\bar{\mathcal{O}}_n^H\rangle\,, \tag{1.2}$$

where $d_{i\to Q\bar{Q}(n)}$ represent the perturbative calculable short-distance coefficients (SDCs) to produce a heavy quark-antiquark pair $Q\bar{Q}$ with quantum number n, and $\langle\bar{\mathcal{O}}_n^H\rangle$ are normalized long-distance matrix elements (LDMEs).[1] The quantum number is usually expressed in spectroscopic notation $n = {}^{2S+1}L_J^{[c]}$, with $c = 1, 8$ respectively for color-singlet state or color-octet state. According to velocity scaling rule [1], $\langle\bar{\mathcal{O}}_n^H\rangle$ is usually suppressed if L is too large. Therefore, the most important states for phenomenological purpose are S-wave and P-wave states. Because LDMEs are supposed to be process independent, they can be determined by fitting experimental data, while SDCs need to be calculated perturbatively.

For both S-wave and P-wave states, all SDCs for single parton FFs are available up to α_s^2 [36–46] (see [47, 48] for a summary and comparison). However, only a few SDCs have been calculated to α_s^3 order, although they are valuable for phenomenological study. Numerical results for SDCs of $g \to Q\bar{Q}({}^3S_1^{[1]}) + X$ were calculated to LO (order α_s^3) in refs. [37, 49–51], including velocity corrections. Analytical results for this process are only available recently [52] by applying multi-loop techniques developed in the past a few years. Using the same techniques, analytical results for SDCs of $g \to Q\bar{Q}({}^1P_1^{[1]}) + X$ at LO (order α_s^3) are also obtained [53]. A more challenging task is the calculation of NLO (order α_s^3)

[1] $\langle\bar{\mathcal{O}}_n^H\rangle$ can be related to the original definition of NRQCD LDME $\langle\mathcal{O}_n^H\rangle$ [1] by the following rules. They are the same if n is color-octet, and $\langle\bar{\mathcal{O}}_n^H\rangle = \langle\mathcal{O}_n^H\rangle/(2N_c)$ if n is color-singlet.

JHEP04(2019)116

SDCs of $g \to Q\bar{Q}({}^1S_0^{[1]}) + X$, which involves not only tree-level diagrams but also one-loop diagrams. Numerical results for this process have been calculated in ref. [54]. Considering the complicity of the calculation, an independent check by another group is badly needed.

As ${}^1S_0^{[1]}$ is the dominant Fock state for $\eta_{c,b}$, the FF $g \to Q\bar{Q}({}^1S_0^{[1]}) + X$ is important to study $\eta_{c,b}$ production at high transverse momentum at LHC [55]. At the LHC, we have even much more data of J/ψ production at high transverse momentum. Theoretical studies [13, 17, 56, 57] show that ${}^1S_0^{[8]}$ channel may be crucial to explain the J/ψ data. To calculate ${}^1S_0^{[8]}$ contribution precisely, we need to calculate the FF $g \to Q\bar{Q}({}^1S_0^{[8]}) + X$ to at least NLO.

In this paper, we aim to calculate NLO SDCs of FFs of $g \to Q\bar{Q}({}^1S_0^{[1]}) + X$ and $g \to Q\bar{Q}({}^1S_0^{[8]}) + X$ to high precision using similar methods in our previous paper [52]. With sufficient numerical precision, analytical results can in principle be extracted by using PSLQ algorithm. The rest of the paper is organized as following. In section 2, we first introduce the definition of SDCs of quarkonium FFs, including projection operators and Feynman rules related to gauge link, and then give the LO results. NLO corrections include real emission Feynman diagrams and one-loop Feynman diagrams, the calculation of them will be presented in section 3 and section 4, respectively. In the calculation, we use integration-by-part (IBP) reduction [58–62] to express both real contributions and virtual contributions in terms of linear combination of a small set of simpler integrals, which are usually called master integrals (MIs). High precision MIs can be obtained by solving differential equations of MIs numerically. Renormalization will be presented in section 5. After renormalization, the obtained SDCs are free of ultraviolet (UV) and infrared (IR) divergences. Final results and discussions will be given in section 6. We find that our results for $g \to Q\bar{Q}({}^1S_0^{[1]}) + X$ seem to be different from that calculated in ref. [54], while our results for $g \to Q\bar{Q}({}^1S_0^{[8]}) + X$ are new. Finally, high precision results and some technical details will be given in appendices.

2 Calculation of LO FFs

2.1 Definitions

The definition of FF from a gluon to a hadron (quarkonium) is given by Collins and Soper [63],

$$D_{g\to H}(z,\mu_0) = \frac{-g_{\mu\nu} z^{D-3}}{2\pi P_c^+ (N_c^2-1)(D-2)} \int_{-\infty}^{+\infty} \mathrm{d}x^- e^{-izP_c^+ x^-} \times \langle 0|G_c^{+\mu}(0)\mathcal{E}^\dagger(0,0,\mathbf{0}_\perp)_{cb}\mathcal{P}_{H(P)}\mathcal{E}(0,x^-,\mathbf{0}_\perp)_{ba}G_a^{+\nu}(0,x^-,\mathbf{0}_\perp)|0\rangle\,, \tag{2.1}$$

where $G^{\mu\nu}$ is the gluon field-strength operator, P and P_c are respectively the momenta of the produced hadron H and the initial-state fragmenting gluon g, and $z = P^+/P_c^+$ is the ratio of momenta along the "+" direction. It is convenient to choose the frame in which the hadron has zero transverse momentum, $P = \left(zP_c^+, m_H^2/(2zP_c^+), \mathbf{0}_\perp\right)$, with $P^2 = 2P^+P^- = m_H^2$. The projection operator $\mathcal{P}_{H(P)}$ is defined by

$$\mathcal{P}_{H(P)} = \sum_X |H(P)+X\rangle\langle H(P)+X|\,, \tag{2.2}$$

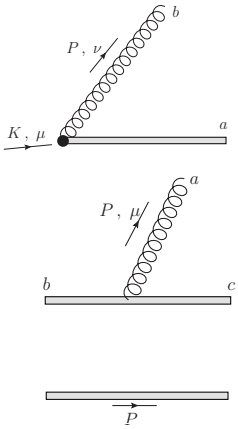

$$= -i\delta^{a\,b}\left(g^{\mu\,\nu} - \frac{P^{\mu}\,n^{\nu}}{K\cdot n}\right)$$

$$= g_s f^{a\,b\,c} n^{\mu}$$

$$= i/(P\cdot n + i\varepsilon)$$

Figure 1. Feynman rules related to the gluon gauge link.

where X sums over all unobserved particles. The gauge link $\mathcal{E}(x^-)$ is an eikonal operator that involves a path-ordered exponential of gluon field operators along a light-like path,

$$\mathcal{E}(0,x^-,\mathbf{0}_\perp)_{ba} = \mathrm{P}\exp\left[+ig_s\int_{x^-}^{\infty}\mathrm{d}z^- A^+(0,z^-,\mathbf{0}_\perp)\right]_{ba}, \tag{2.3}$$

where $g_s = \sqrt{4\pi\alpha_s}$ is the QCD coupling constant and $A^\mu(x)$ is the matrix-valued gluon field in the adjoint representation: $[A^\mu(x)]_{ac} = if^{abc}A^\mu_b(x)$.

From this definition, we can derive Feynman rules related to gauge link, which are shown in figure 1, where $n = (0, 1^-, \mathbf{0}_\perp)$, K and P denote momenta, μ and ν denote Lorentz indexes, and a, b and c denote color indices.

With these Feynman rules, we can obtain the amplitude of all Feynman diagrams denoted as $\mathcal{M}_{\lambda_Q\lambda_{\bar{Q}}\lambda_0\lambda_i}(P, k_i, m_Q)$, where λ_Q and $\lambda_{\bar{Q}}$ are respectively spins of produced on-shell heavy quark and heavy antiquark, λ_0 and λ_i ($i = 1, 2, \dots$) are spins of the initial-state virtual gluon and final-state unobserved light particles, respectively, k_i are the momenta of final-state light particles, and m_Q is the heavy quark mass. For the processes of gluon fragmenting to S-wave quarkonium, the relative momentum between the $Q\bar{Q}$ pair can be chosen as 0 directly at the lowest order in velocity expansion, and thus it does not appear in the amplitude. If we project the free $Q\bar{Q}$ pair to specific states ${}^1S_0^{[1]}$ or ${}^1S_0^{[8]}$, we have

$$\mathcal{M}_{\lambda_0\lambda_i}(P, k_i, m_Q) = \mathrm{Tr}\left[\Gamma_c\Gamma_5\mathcal{M}_{\lambda_Q\lambda_{\bar{Q}}\lambda_0\lambda_i}(P, k_i, m_Q)\right], \tag{2.4}$$

where $\Gamma_c\,, \Gamma_5$ are the projection operators defined as

$$\begin{aligned}
\Gamma_{c=1} &= \frac{1}{\sqrt{N_c}}\,,\\
\Gamma_{c=8} &= \frac{\sqrt{2}T^a}{\sqrt{N_c^2-1}}\,,\\
\Gamma_5 &= \frac{1}{\sqrt{M(M/2+m_Q)}}(\not{P}/2 - m_Q)\frac{M-\not{P}}{2M}\gamma^5\frac{M+\not{P}}{2M}(\not{P}/2-m_Q)\,,
\end{aligned} \tag{2.5}$$

JHEP04(2019)116

where $P^2 = M^2 = 4m_Q^2$. By summing over spin and color of initial-state and final-state particles, we get the squared amplitude

$$|\mathcal{M}(P, k_i, m_Q)|^2 = \overline{\sum} |\mathcal{M}_{\lambda_0 \lambda_i}(P, k_i, m_Q)|^2 \,. \tag{2.6}$$

Then the SDCs for gluon fragmenting to spin-singlet S-wave quarkonium can be written as

$$d(z) = N_{\rm CS} \int \mathrm{d}\Phi \, |\mathcal{M}(P, k_i, m_Q)|^2 \,, \tag{2.7}$$

where $N_{\rm CS} = \frac{z^{D-2}}{(N_c^2-1)(D-2)}$ with $D = 4 - 2\epsilon$ is the space-time dimension, and final-state phase space is defined as

$$\begin{aligned} \mathrm{d}\Phi &= \frac{1}{S}\delta\left(z - \frac{P^+}{P_c^+}\right)(2\pi)^D \delta^D\left(P_c - P - \sum_i k_i\right) \frac{\mathrm{d}^D P_c}{(2\pi)^D} \prod_i \frac{\mathrm{d}k_i^+}{4\pi k_i^+} \frac{\mathrm{d}^{D-2} k_{i\perp}}{(2\pi)^{D-2}} \theta(k_i^+) \\ &= \frac{P^+}{z^2 S}\delta\left(\frac{1-z}{z} P^+ - \sum_i k_i^+\right) \prod_i \frac{\mathrm{d}k_i^+}{4\pi k_i^+} \frac{\mathrm{d}^{D-2} k_{i\perp}}{(2\pi)^{D-2}} \theta(k_i^+) \end{aligned} \tag{2.8}$$

where S is the symmetry factor for final-state particles.

To be convenient, we extract the dependence on m_Q explicitly by rescaling momenta in the delta function in eq. (2.8) by M,

$$\hat{P} = \frac{P}{M} \,, \qquad \hat{k}_i = \frac{k_i}{M} \,, \qquad \hat{m}_Q = \frac{m_Q}{M} = \frac{1}{2} \,. \tag{2.9}$$

Thus the phase space in eq. (2.8) changes to

$$\mathrm{d}\Phi = M^{n(D-2)} \mathrm{d}\hat{\Phi} \,, \tag{2.10}$$

where n is the number of final-state light particles, and $\mathrm{d}\hat{\Phi}$ is similar to $\mathrm{d}\Phi$ by changing all momenta to the dimensionless ones. If we further denote

$$\hat{\mathcal{M}}_{\lambda_0 \lambda_i}(\hat{P}, \hat{k}_i, m_Q) = M^{n(D-2)/2} \mathcal{M}_{\lambda_0 \lambda_i}(M\hat{P}, M\hat{k}_i, M\hat{m}_Q) \,, \tag{2.11}$$

we get a similar relation as that in eq. (2.7),

$$d(z) = N_{\rm CS} \int \mathrm{d}\hat{\Phi} \, \left|\hat{\mathcal{M}}(\hat{P}, \hat{k}_i, \hat{m}_Q)\right|^2, \tag{2.12}$$

which means that the same SDCs can be obtained by replacing all momenta by their corresponding rescaled ones. In the rest of the paper, we will only use the rescaled momenta, but omitting the "ˆ" for simplicity.

2.2 LO SDCs

The Feynman diagrams of gluon fragmenting into ${}^1S_0^{[1]}$ or ${}^1S_0^{[8]}$ $Q\bar{Q}$ at LO in α_s are shown in figure 2. From the definition above, the calculation of LO SDCs involves integrals of the form

$$\int \mathrm{d}\Phi_{\rm Born} \frac{1}{k \cdot P + a} \,, \tag{2.13}$$

JHEP04(2019)116

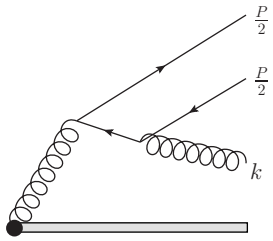

Figure 2. One of the two Feynman diagrams of gluon fragmenting into ${}^1S_0^{[1]}$ or ${}^1S_0^{[8]}$ $Q\bar{Q}$ at LO in α_s. Another diagram can be obtained by permuting the heavy quark and anti-quark.

where a equals 0 or 1/2, k is the momentum of the emitted gluon with $k^+ = (1-z)P^+/z$ and $k^- = k_\perp^2/(2k^+)$, and

$$\int \mathrm{d}\Phi_{\mathrm{Born}} = \frac{1}{4\pi z(1-z)} \int \frac{\mathrm{d}^{D-2}k_\perp}{(2\pi)^{D-2}}\,. \tag{2.14}$$

These integrals can be performed easily.

Then we get LO SDCs:

$$d_{\mathrm{LO}}^{[1]}(z) = \frac{\alpha_s^2}{2(1-\epsilon)N_c m_Q^3}\left(\frac{\pi\mu_r^2}{m_Q^2}\right)^\epsilon d_{\mathrm{LO}}(z)\,, \tag{2.15}$$

$$d_{\mathrm{LO}}^{[8]}(z) = \frac{\alpha_s^2(N_c^2-4)}{4(1-\epsilon)N_c(N_c^2-1)m_Q^3}\left(\frac{\pi\mu_r^2}{m_Q^2}\right)^\epsilon d_{\mathrm{LO}}(z)\,, \tag{2.16}$$

where μ_r is the renormalization scale, $d_{\mathrm{LO}}^{[1]}$ and $d_{\mathrm{LO}}^{[8]}$ respectively denote SDCs of gluon fragmenting into ${}^1S_0^{[1]}$ and ${}^1S_0^{[8]}$ states, and

$$d_{\mathrm{LO}}(z) = \Gamma(\epsilon)(2\epsilon-1)(1-z)^{-2\epsilon}\left[\big(z(\epsilon^2-\epsilon+2)-2\big)(1-z)^\epsilon + 2(z-1)(z\epsilon-1)\right], \tag{2.17}$$

with

$$d_{\mathrm{LO}}^{(0)}(z) = \lim_{\epsilon\to 0} d_{\mathrm{LO}}(z) = (3-2z)z + 2(1-z)\ln(1-z)\,. \tag{2.18}$$

The color-singlet result and color-octet result are consistent with refs. [54] and [45], respectively.

3 Real NLO corrections

3.1 Reduction to MIs

Real NLO corrections to FFs of $g \to Q\bar{Q}({}^1S_0^{[1,8]}) + X$ come from Feynman diagrams with two real light particles in the final state, either two gluons or a light quark-antiquark ($q\bar{q}$) pair. Feynman diagrams with two gluons emission are shown in figure 3, while those with $q\bar{q}$ pair emission are shown in figure 4.

SDCs can be expressed as linear combinations of integrals of the form

$$\begin{aligned}\int \mathrm{d}\Phi_{\mathrm{real}} \prod_i \frac{1}{E_i^{a_i}} = \\ \frac{P\cdot n}{2z^2}\int \frac{\mathrm{d}^D k_1}{(2\pi)^{D-1}}\frac{\mathrm{d}^D k_2}{(2\pi)^{D-1}}\delta_+(k_1^2)\delta_+(k_2^2)\delta\left(k_1\cdot n + k_2\cdot n - \frac{1-z}{z}P\cdot n\right)\prod_i \frac{1}{E_i^{a_i}}\,,\end{aligned} \tag{3.1}$$

JHEP04(2019)116

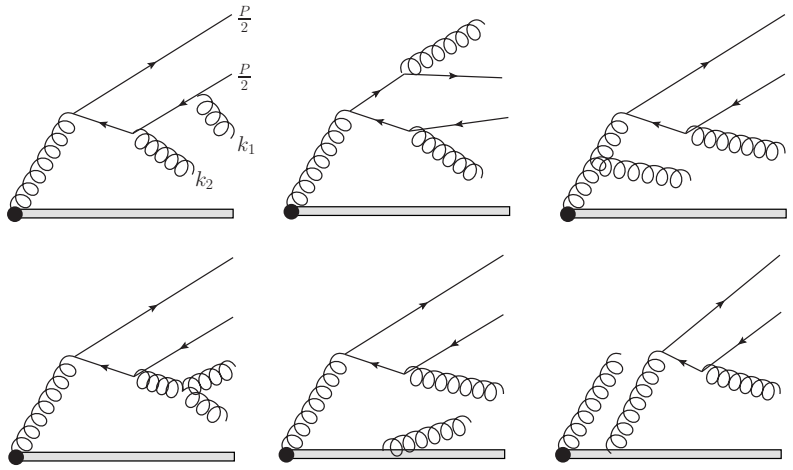

Figure 3. Typical Feynman diagrams for $g \to Q\bar{Q}({}^1S_0^{[1,8]}) + gg$. The other diagrams can be obtained by permuting the heavy quark and anti-quark or the two emitted gluons.

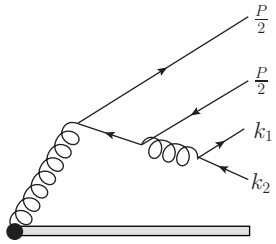

Figure 4. One of the two Feynman diagrams for $g \to Q\bar{Q}({}^1S_0^{[1,8]}) + q\bar{q}$. Another diagram can be obtained by permuting the heavy quark and anti-quark.

where a_i are integers, k_1 and k_2 are momenta of the final-state light particles, the phase space $\mathrm{d}\Phi_{\mathrm{real}}$ is defined in eq. (2.8) with $S = 2$, and

$$\begin{aligned}
&E_1 = k_1\cdot k_2\,, \qquad E_2 = k_1\cdot P\,, \qquad E_3 = k_2\cdot P\,, \qquad E_4 = 2\,k_1\cdot P+1\,, \qquad E_5 = 2\,k_2\cdot P+1\,,\\
&E_6 = 2\,k_1\cdot k_2+k_1\cdot P+k_2\cdot P\,, \qquad\qquad E_7 = 2\,k_1\cdot k_2+2\,k_1\cdot P+2\,k_2\cdot P+1\,,\\
&E_8 = k_1\cdot n\,, \qquad E_9 = k_1\cdot n+P\cdot n\,, \qquad E_{10} = k_2\cdot n\,, \qquad E_{11} = k_2\cdot n+P\cdot n\,.
\end{aligned} \tag{3.2}$$

In eq. (3.1), we safely ignore infinitesimal imaginary parts in denominators because $E_i (i = 1, \cdots 11)$ are positive-definite and that SDCs are well regularized by dimensional regularization. The later condition implies that only the region where all $E_i (i = 1, \cdots 11)$ are not too small can contribute to the phase space integration. Note that, for $q\bar{q}$ pair emission, although the symmetry factor should be 1, we can also express the SDCs as linear combinations of integrals in eq. (3.1).

To take advantage of multi-loop techniques, we express delta functions by propagator denominators,

$$(2\pi)\delta(x) = \lim_{\eta\to 0^+}\left(\frac{i}{x+i\eta} + \frac{-i}{x-i\eta}\right). \tag{3.3}$$

JHEP04(2019)116

We replace the three delta functions in eq. (3.1) following the above rule, and denote

$$E_{12} = k_1^2\,, \qquad E_{13} = k_2^2\,, \qquad E_{14} = k_1\cdot n + k_2\cdot n - \frac{1-z}{z} P\cdot n\,. \tag{3.4}$$

Then each phase space integral in eq. (3.1) is translated to 8 loop integrals, with either positive or negative infinitesimal imaginary parts in new denominators.

If we forget about infinitesimal imaginary parts in denominators for the moment, we need to deal with loop integrals

$$\int \frac{\mathrm{d}^D k_1}{(2\pi)^D} \frac{\mathrm{d}^D k_2}{(2\pi)^D} \prod_{i=1}^{14} \frac{1}{E_i^{a_i}} \tag{3.5}$$

with integers a_i, which can be expressed in terms of corresponding simpler MIs by using IBP reduction [58–62]. MIs are also the same kind of integrals, but usually with smaller a_i. Note that, we can always choose MIs with powers of E_{12}, E_{13} and E_{14} being no larger than 1. For MIs with integrand involving $\frac{1}{E_{12}}$, we can replace the denominator by $\delta_+(k_1^2)$ considering the relation eq. (3.3), while for MIs with integrand $E_{12}^{-a_{12}}$ ($a_{12} \leq 0$) we can set it to zero. Similar replacement can be done for E_{13} and E_{14}. Therefore, all MIs for loop integration are changed back to corresponding MIs for phase space integration defined in eq. (3.1). Once these MIs are also calculated, we obtain final results of real corrections.

In the above procedure, we actually assume that IBP reduction relations are independent of infinitesimal imaginary parts in denominators. This assumption, unfortunately, does not always hold. If one or more integrals cannot be fully regularized by dimensional regularization, one may get wrong final results. In the appendix A, we will discuss this problem in more details, and then propose a solution. Eventually, the above procedure is justified with a small modification.

3.2 Calculation of MIs

To calculate these MIs, we use differential equations (DEs) method [64–76], which has also been used in our previous paper [52] to calculate SDCs of $g \to Q\bar{Q}(^3S_1^{[1]}) + X$. We get 95 MIs using the IBP reduction program FIRE5 [62], without using the symmetry rules. We set up DEs by first differentiating these MIs $I_k (k = 1, \ldots, 95)$ with respect to z, and then reducing the resulted integrals to MIs again by using IBP reduction, which results in

$$\frac{\mathrm{d}\boldsymbol{I}(\epsilon, z)}{\mathrm{d}z} = A(\epsilon, z)\boldsymbol{I}(\epsilon, z)\,, \tag{3.6}$$

where $\boldsymbol{I}$ represents the vector of MIs I_k, and A is a 95×95 matrix whose elements are rational functions of z and ϵ. Having the DEs, we also need boundary conditions of I_k to fully determine these MIs. We choose the boundary at $z \to 1$, and calculate the boundary conditions in appendix C.

With boundary conditions, we can solve the DEs to obtain MIs at any value of z. One possible choice is to solve the DEs analytically, which can be done by transforming DEs into canonical form (or ϵ-form) [68, 69]. In this way, we successfully express MIs in terms of Goncharov polylogarithms (GPLs) [77]. All obtained GPLs have weights at

JHEP04(2019)116

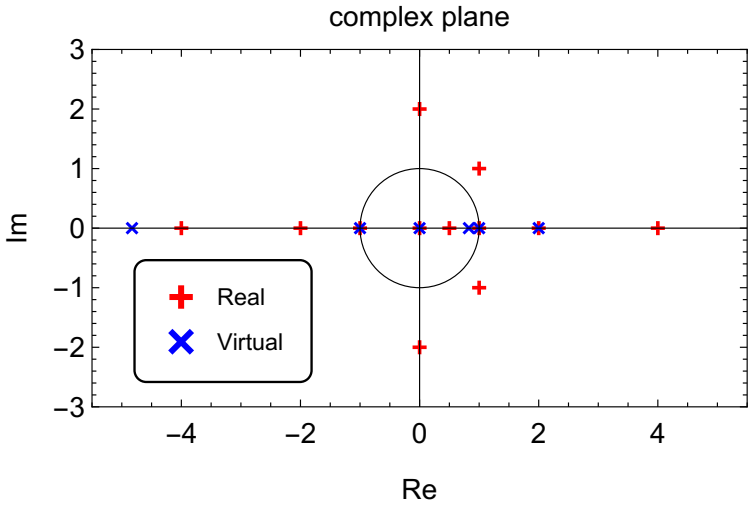

Figure 5. Singularities of DEs of MIs for both $g \to Q\bar{Q}(^1S_0^{[1]}) + X$ and $g \to Q\bar{Q}(^1S_0^{[8]}) + X$. Plus signs denote singularities encountered in real corrections while multiplication signs denote singularities encountered in virtual corrections.

most three, and they can be expressed in terms of logarithms and classical polylogarithms $\mathrm{Li}_n(z), (n \leq 3)$ [78]. Even though, the obtained analytical expression is too long to present in this paper. Furthermore, for virtual correction, boundary conditions are hard to calculate analytically.

Another choice is to solve DEs numerically, which is a well-studied mathematical problem. DEs can help to do asymptotic expansions of MIs around any point $z = z_0$. Because Feynman integrals have Feynman parametric representation, their asymptotic expansions have the form (see e.g. ref. [79])

$$I_k(z,\epsilon)|_{z_0} = \sum_s \sum_{i=0}^{n_s} (z-z_0)^s \ln^i(z-z_0) \sum_{j=0}^{\infty} I_k^{s\,i\,j}(\epsilon)(z-z_0)^j, \tag{3.7}$$

where s is a linear function of ϵ, n_s is an integer determined by s, $I_k^{s\,i\,j}(\epsilon)$ are functions of ϵ, and the radius of convergence of the summation over j is usually determined by the nearest singular point. For the special case when z_0 is an analytical point, we have $s = n_s = 0$. When z_0 is a singular point, different values of s and i correspond to different regions of MIs, which are independent of each other. Therefore, each region satisfies the same DEs as the original MIs, and the DEs can generate recurrence relations to express $I_k^{s\,i\,j}(\epsilon)$ in terms of $I_k^{s\,0\,0}(\epsilon)$ for each fixed s, i and ϵ. It implies that, when calculating boundary conditions in appendix C, we only need to calculate $I_k^{s\,0\,0}(\epsilon)$ for each region. In practice, as we are only interested in MIs up to a fixed order in ϵ expansion, we will do a Laurent expansion of ϵ in both $(z-z_0)^s$ and $I_k^{s\,i\,j}(\epsilon)$.

As it is clear, singular points play important role in the procedure of solving DEs numerically. There are 12 singular points in the DEs (3.6) for real corrections, which are located at $z = 0, 1/2, \pm 1, \pm 2, \pm 4, \pm 2i, 1 \pm i$, as shown in figure 5. For the interested physical region $0 \leq z \leq 1$, the only relevant singularities are $z = 0, 1/2, 1$, and all other

JHEP04(2019)116

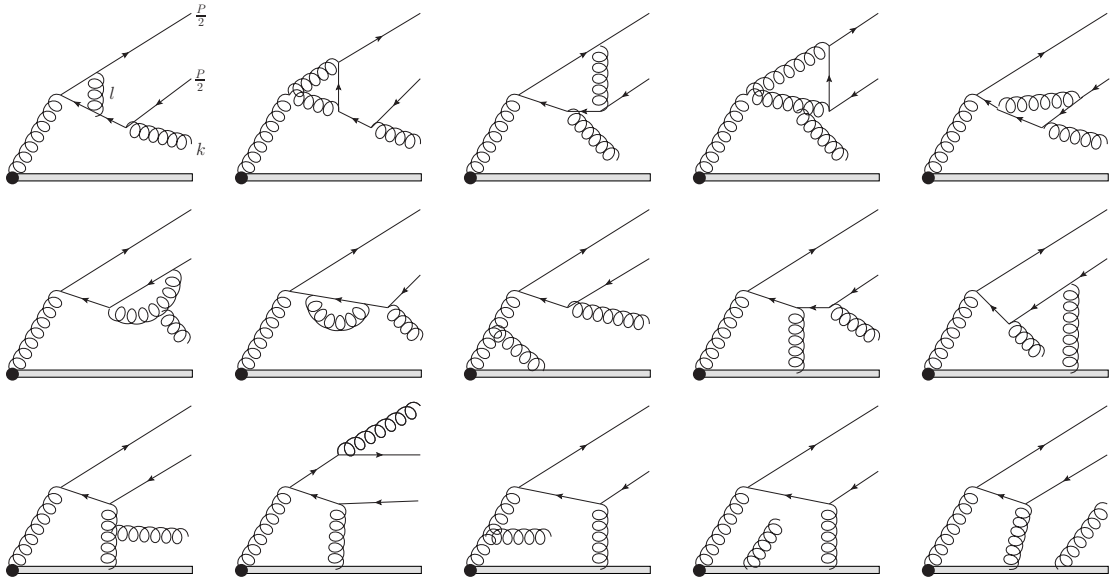

Figure 6. Some typical Feynman diagrams of the virtual NLO correction for gluon fragmenting into ${}^1S_0^{[1]}$ or ${}^1S_0^{[8]}$ $Q\bar{Q}$. The other diagrams are either self-energy diagrams for external legs (including initial virtual gluon), or they can be obtained by permuting the heavy quark and anti-quark.

singularities are far enough from the physical region. Among these three singularities, the point $z = 1/2$ is in fact a removable singularity. However, as we will discuss in appendix B, this singularity determines the radius of convergence of the asymptotic expansion at $z = 0$ and 1. We thus estimate values of MIs in regions $0 \sim 1/4$, $1/4 \sim 3/4$ and $3/4 \sim 1$ respectively by the asymptotic expansions of MIs at $z = 0, 1/2$ and 1. For example, if we want to obtain values in the physical region with precision about 15 digits, we should calculate the expansion in eq. (3.7) with j to as large as 50.

4 Virtual NLO corrections

Some diagrams that contributed to virtual NLO corrections to FFs of $g \to Q\bar{Q}({}^1S_0^{[1,8]}) + X$ are shown in figure 6. The other diagrams are either self-energy diagrams for external legs (including initial virtual gluon), or they can be obtained by permuting the heavy quark and anti-quark.

SDCs of the virtual corrections can be expressed as linear combination of integrals of the form

$$\int \mathrm{d}\Phi_{\mathrm{loop}} \int \frac{\mathrm{d}^D l}{(2\pi)^D} \prod_i \frac{1}{F_i^{a_i}} = \frac{P\cdot n}{z^2} \int \frac{\mathrm{d}^D k}{(2\pi)^{D-1}} \frac{\mathrm{d}^D l}{(2\pi)^D} \delta_+(k^2)\delta\left(k\cdot n - \frac{1-z}{z} P\cdot n\right) \prod_i \frac{1}{F_i^{a_i}}\,, \tag{4.1}$$

where $z = P^+/(k^+ + P^+)$, a_i are integers, k is the momentum of the final-state gluon, l is

JHEP04(2019)116

the loop momenta, and

$$F_1 = k\cdot P, \quad F_2 = 2\,k\cdot P + 1\,, \quad F_3 = l^2, \quad F_4 = (l+k)^2, \quad F_5 = (l+P)^2, \quad F_6 = \left(l+\frac{P}{2}\right)^2 - \frac{1}{4}\,,$$
$$F_7 = \left(l-\frac{P}{2}\right)^2 - \frac{1}{4}\,, \quad F_8 = \left(l+k+\frac{P}{2}\right)^2 - \frac{1}{4}\,, \quad F_9 = (l+k+P)^2, \quad F_{10} = l\cdot n\,. \tag{4.2}$$

Similar to real corrections, by replacing δ functions using eq. (3.3), integrals in eq. (4.1) can be reduced to corresponding simpler MIs, the number of which is 66. DEs for these MIs can also be set up.

As for real corrections, asymptotic expansion of virtual-correction MIs at any point $z = z_0$ can be obtained in the form of eq. (3.7) with the help of DEs, once we have boundary conditions for these DEs. The DEs have 6 singularities in the complex-z plane, $z = 0, \pm 1, 2, 2(\pm\sqrt{2}-1)$, as shown in figure 5. For the physical region, the relevant poles are $z = 0, 2(\sqrt{2}-1), 1$, among which $z = 2(\sqrt{2}-1)$ is a removable singularity. We will discuss in appendix B that this removable singularity does not affect the radius of convergence of asymptotic expansion at $z = 1$, although it can decrease the precision if we estimate values for $z < 2(\sqrt{2}-1)$ from the asymptotic expansion at $z = 1$. The later problem has no impact if boundary conditions can be calculated to sufficient high precision, which is indeed the case as we will explain later. Therefore, virtual-correction MIs in regions $0 \sim 1/4$, $1/4 \sim 3/4$ and $3/4 \sim 1$ can be respectively estimated by the asymptotic expansions of MIs at $z = 0, 1/2$ and 1, where we introduce an expansion at a non-singular point $z = 1/2$ so that the combination of real corrections and virtual corrections can be expressed by a single piecewise function.

Finally, let us discuss how to obtain boundary conditions for DEs of virtual-correction MIs. We find that, if we choose boundary conditions at $z \to 1$, calculation of these MIs either analytically or numerically to high precision is very hard. The method proposed in refs. [75, 76] provides a way to calculate MIs numerically to very high precision at any non-singular point z, which we will explain in appendix D. With this method, we can not only provide boundary conditions for DEs, but also do a self-consistent check. To this purpose, we use this method to calculate MIs at two points, say $z = z_1$ and z_2. With results at $z = z_1$ as boundary conditions, the DEs can give prediction for MIs at $z = z_2$, and the later values can be compared with the values obtained by this method. In our work, we have done this self-consistent check, and find a perfect agreement.

5 Renormalization

Bare quantities of fields Ψ_b and A_b, coupling constant g_{sb}, and heavy quark mass m_{Qb} are related to corresponding renormalized ones by the renormalization constants $\delta_2\,, \delta_3\,, \delta_g$ and δ_m,

$$\Psi_b = (1+\delta_2)^{1/2}\Psi\,, \qquad A_b^\mu = (1+\delta_3)^{1/2}A^\mu\,, \qquad g_{sb} = (1+\delta_g)g_s\,, \qquad m_{Qb} = (1+\delta_m)m_Q\,. \tag{5.1}$$

JHEP04(2019)116

In this paper, we choose $\overline{\text{MS}}$ renormalization scheme for the coupling constant, and choose on-shell renormalization scheme for gluon field, heavy quark field and heavy quark mass. It is convenient to rescale the renormalization constants as following

$$\delta_i = \frac{\alpha_s}{\pi}\Gamma(1+\epsilon)\left(\frac{\pi\mu_r^2}{m_Q^2}\right)^{\epsilon}\hat{\delta}_i\,, \tag{5.2}$$

with

$$\begin{aligned}
\hat{\delta}_2 &= -\frac{C_F}{4}\left(\frac{1}{\epsilon_{\text{UV}}}+\frac{2}{\epsilon_{\text{IR}}}+4+6\ln 2\right),\\
\hat{\delta}_3 &= \left(\frac{5}{12}N_c-\frac{1}{6}n_f\right)\left(\frac{1}{\epsilon_{\text{UV}}}-\frac{1}{\epsilon_{\text{IR}}}\right),\\
\hat{\delta}_g &= -\frac{b_0}{4}\left(\frac{1}{\epsilon_{\text{UV}}}-\ln\frac{\mu_r^2}{4m_Q^2}\right),\\
\hat{\delta}_m &= -\frac{3C_F}{4}\left(\frac{1}{\epsilon_{\text{UV}}}+\frac{4}{3}+2\ln 2\right),
\end{aligned} \tag{5.3}$$

where $b_0 = (11N_c - 2n_f)/6$.

Summing over all counter terms, we obtain

$$\int \mathrm{d}\Phi_{\text{Born}}\left(\delta_2+2\delta_g+\frac{\delta_m}{2k\cdot P}\right)|\mathcal{M}_{\text{LO}}|^2, \tag{5.4}$$

where $|\mathcal{M}_{\text{LO}}|^2$ is the squared amplitude at LO in α_s, and $\mathrm{d}\Phi_{\text{Born}}$ is defined in eq. (2.14). This integral can be calculated easily.

Besides, we need to renormalize the operator defining the FF. In $\overline{\text{MS}}$ scheme, the counter term gives

$$d^{[1/8]}_{\text{Operator}}(z) = -\frac{\alpha_s}{2\pi}\frac{\Gamma(1+\epsilon)}{\epsilon}\left(\frac{4\pi\mu_r^2}{\mu_f^2}\right)^{\epsilon}\int_z^1\frac{\mathrm{d}y}{y}P_{gg}(y)d^{[1/8]}_{\text{LO}}\left(\frac{z}{y}\right), \tag{5.5}$$

where μ_f is the factorization scale, $d^{[1/8]}_{\text{LO}}(z)$ are given respectively in eq. (2.15) and eq. (2.16), and the Altarelli-Parisi splitting function $P_{gg}(z)$ is

$$P_{gg}(z) = b_0\,\delta(1-z)+2N_c\left(\frac{z}{(1-z)_+}+\frac{1-z}{z}+z(1-z)\right). \tag{5.6}$$

6 Results and discussion

6.1 Final results

Summing over real corrections, virtual corrections and all counter terms, we obtain finite results at NLO for both FFs. The results can be expressed in terms of piecewise functions,

$$\begin{aligned}
d^{[1]}_{\text{NLO}}(z) &= \frac{\alpha_s^3}{2\pi N_c m_Q^3}\times\left(d^{[1]}(z)+\ln\left(\frac{\mu_r^2}{4m_Q^2}\right)b_0\,d^{(0)}_{\text{LO}}(z)+\ln\left(\frac{\mu_f^2}{4m_Q^2}\right)f(z)\right),\\
d^{[8]}_{\text{NLO}}(z) &= \frac{\alpha_s^3(N_c^2-4)}{4\pi N_c(N_c^2-1)m_Q^3}\times\left(d^{[8]}(z)+\ln\left(\frac{\mu_r^2}{4m_Q^2}\right)b_0\,d^{(0)}_{\text{LO}}(z)+\ln\left(\frac{\mu_f^2}{4m_Q^2}\right)f(z)\right),
\end{aligned} \tag{6.1}$$

JHEP04(2019)116

where b_0 is given below eq. (5.3), $d_{\rm LO}^{(0)}(z)$ is given in eq. (2.18),

$$f(z) = -\frac{n_f}{6} d_{\rm LO}^{(0)}(z) + N_c \bigg(-2(z+2){\rm Li}_2(z) - 2(z-1)\ln^2(1-z) + 2(z-1)\ln(z)\ln(1-z) + (z-4)z\ln(z) - \frac{(2z+1)(9z^2-5z-6)\ln(1-z)}{6z} + \frac{46z^3+(8\pi^2-3)z^2+4(\pi^2-9)z+4}{12z} \bigg), \tag{6.2}$$

and

$$d^{[1/8]}(z) = \begin{cases} -\dfrac{N_c}{2z} + \displaystyle\sum_{i=0}^{2}\sum_{j=0}^{\infty} \ln^i z\,(2z)^j \left(A_{ij}^f\, n_f + A_{ij}^{[1/8]}\, N_c + \frac{A_{ij}^N}{N_c} \right), & \text{for } 0 < z < \frac{1}{4} \\ \displaystyle\sum_{j=0}^{\infty} (2z-1)^j \left(B_j^f\, n_f + B_j^{[1/8]}\, N_c + \frac{B_j^N}{N_c} \right), & \text{for } \frac{1}{4} \le z \le \frac{3}{4} \\ \displaystyle\sum_{i=0}^{3}\sum_{j=0}^{\infty} \ln^i(1-z)\,(2-2z)^j \left(C_{ij}^f\, n_f + C_{ij}^{[1/8]}\, N_c + \frac{C_{ij}^N}{N_c} \right), & \text{for } \frac{3}{4} < z < 1 \end{cases} . \tag{6.3}$$

The coefficients A_{ij}^k, B_j^k, C_{ij}^k can be evaluated numerically to very high precision, then analytical results can be obtained by fitting numerical results using PSLQ algorithm. For example, with 20-digit precision, we get

$$A_{00}^{[1]} = A_{00}^{[8]} = 17 - \frac{11\zeta(3)}{8} - \frac{13\pi^2}{12} + \ln^2 2 - \frac{\pi^2}{4}\ln 2\,. \tag{6.4}$$

In practice, however, numerical results with high precision will be sufficient. In appendix E, we present these coefficients up to $j = 40$ with 14 digits for each coefficient. With these numerical results, we can calculate $d_{\rm NLO}^{[1/8]}(z)$ to more than 12-digit precision for any value of z. To obtain results with 160-digit precision at any value of z, we attach an ancillary file with these coefficients calculated up to $j = 530$.

6.2 Numerical results

To see the effects of NLO corrections, we choose parameters the same as that in ref. [54], with $m_b = 4.75\,\text{GeV}$, $N_c = 3$, $n_f = 4$, and $\alpha_s(\mu_r = 2m_b) = 0.181$. In figure 7, we plot the curves of LO FFs and LO+NLO FFs with $\mu_r = \mu_f = 2m_b$. To show color-singlet FFs and color-octet FFs in the same figure, we introduce overall factors $c^{[1]} = 6m^3$ and $c^{[8]} = 96m^3/5$ for them, respectively. We find that our result of NLO FF of $g \to Q\bar{Q}(^1S_0^{[1]}) + X$ has some differences from that obtained in ref. [54], especially when $z \to 0$. With $\mu_r = \mu_f = 2m_b$, we also provide K-factors (the ratio of LO+NLO over LO) of some special values of z in table 1, where we find that K-factors are very significant for most values of z.

As shown in eq. (6.3), NLO FFs are negative and divergent at both $z = 0$ and $z = 1$, with leading behavior $1/z$ at $z \to 0$ and $\ln^2(1-z)$ at $z \to 1$. Thus total fragmenting probability obtained by integrating NLO FFs over z from 0 to 1 are divergent. The divergence at $z \to 0$ is not a big problem because physical cross sections are obtained by convolving

JHEP04(2019)116

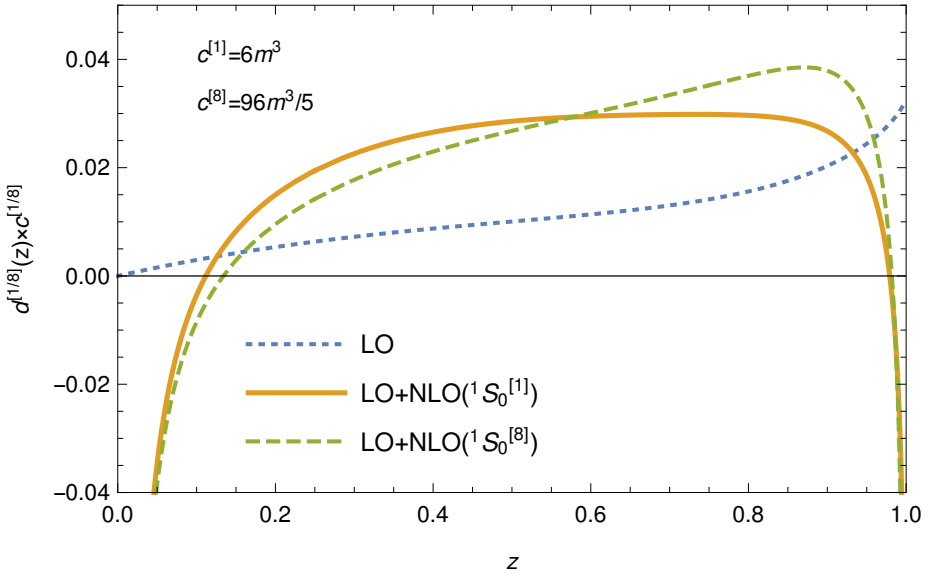

Figure 7. SDCs of the fragmentation functions of $g \to b\bar{b}(^1S_0^{[1]})$ and $g \to b\bar{b}(^1S_0^{[8]})$ at LO and NLO. The dotted line is for $d_{\rm LO}^{[1]}(z)\times(6m_b^3)$ or $d_{\rm LO}^{[8]}(z)\times(96m_b^3/5)$, the solid line is for $\left(d_{\rm LO}^{[1]}(z)+d_{\rm NLO}^{[1]}(z)\right)\times(6m_b^3)$ and the dashed line is for $\left(d_{\rm LO}^{[8]}(z)+d_{\rm NLO}^{[8]}(z)\right)\times(96m_b^3/5)$, with scale choices $\mu_r=\mu_f=2m_b$. The superscript [1] or [8] respectively denotes the color-singlet or color-octet states of $b\bar{b}$.

z	$K^{[1]}$	$K^{[8]}$	z	$K^{[1]}$	$K^{[8]}$
0.05	−22.2154523437	−24.6733986814	0.55	2.72527357574	2.66250417113
0.10	−1.19896707966	−2.87199122365	0.60	2.59460446402	2.64623824982
0.15	1.96212951638	0.686093914799	0.65	2.44998117224	2.61539737443
0.20	2.80788837291	1.79077857154	0.70	2.28930766059	2.56549304191
0.25	3.06753043346	2.24294113774	0.75	2.10880071058	2.48839147108
0.30	3.12597786091	2.45762890747	0.80	1.90118848020	2.36993271047
0.35	3.10100074972	2.56808157787	0.85	1.65072948968	2.18335185168
0.40	3.03565411189	2.62635170085	0.90	1.31711318345	1.86698847168
0.45	2.94726594487	2.65539830293	0.95	0.755737935988	1.20834068587
0.50	2.84294512935	2.66590375106	0.99	−0.694039121672	−0.839542885588

Table 1. K-factors at different values of z. The superscript [1] or [8] respectively denotes the color-singlet or color-octet states of $b\bar{b}$.

FFs with partonic hard parts, which behave as z^n in the small z region with n usually larger than 4.[2] Therefore, the small z region has negligible contributions to physical cross sections. The divergence at $z \to 1$ region, on the other hand, means that perturbative calculation in this region is not good. We leave the study of resummation of FFs in the $z \to 1$ region for future works.

[2]According to naive mass dimensional counting, partonic differential cross section $d\sigma/dp_T^2$ behaves as z^4/p_T^4, where p_T/z is the transverse momentum of the fragmenting parton. Due to anomalous dimension from α_s and PDFs, differential cross sections are further suppressed at small z.

JHEP04(2019)116

State	SDCs$*c^{[1/8]}$	z^2	z^4	z^6
	LO ($\times 10^{-3}$)	5.55116944444	3.85331761905	2.99519856859
$^1S_0^{[1]}$	LO+NLO ($\times 10^{-3}$)	7.54577896198	3.90413390636	2.31890675630
	K-factor	1.35931339108	1.01318767159	0.774208021001
$^1S_0^{[8]}$	LO+NLO ($\times 10^{-3}$)	8.94021475091	4.99398540596	3.12511443983
	K-factor	1.61051015293	1.29602225917	1.04337471064

Table 2. Moments and K-factor of SDCs.

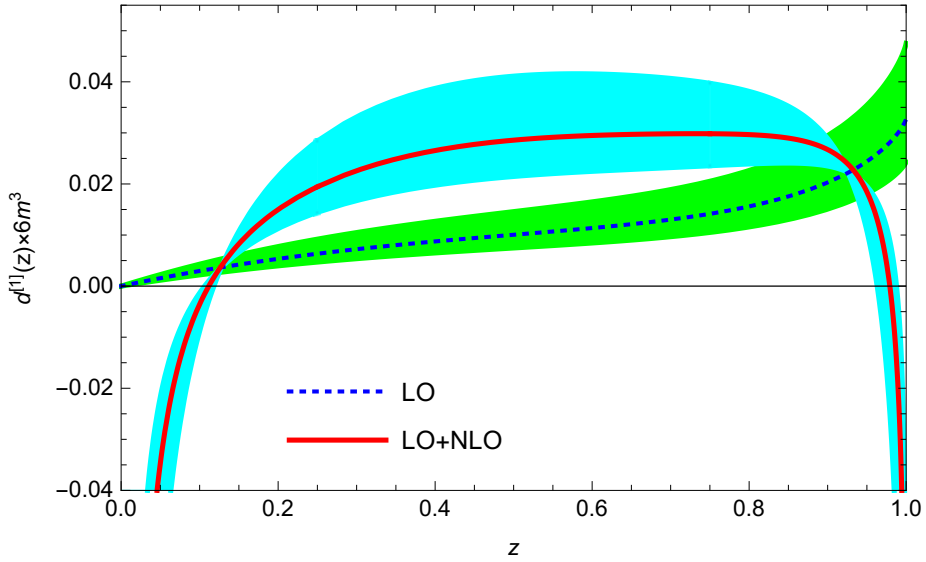

Figure 8. SDCs of the fragmentation function of $g \to b\bar{b}(^1S_0^{[1]}) + X$ at LO and NLO. The dotted line is for $d^{[1]}_{\rm LO}(z) \times (6m_b^3)$, while the solid line is for $\left(d^{[1]}_{\rm LO}(z) + d^{[1]}_{\rm NLO}(z)\right) \times (6m_b^3)$, with scale choices $\mu_r = \mu_f = 2m_b$. The bands are obtained by varying the renormalization scale μ_r by a factor of 2.

To estimate the impact of our NLO calculation on physical cross sections, we calculate the moments of FFs,

$$\int_0^1 \mathrm{d}z\, z^n \left(d^{[1/8]}_{\rm LO}(z) + d^{[1/8]}_{\rm NLO}(z)\right) * c^{[1/8]}, \tag{6.5}$$

with numerical results shown in table 2 for $n = 2, 4, 6$. We find that, unlike K-factors for fixed z, K-factors of 4-th moments and 6-th moments are moderate.

The sensitivities of LO and LO+NLO FFs with respective to the renormalization scale μ_r are illustrated in figure 8 for $g \to Q\bar{Q}(^1S_0^{[1]}) + X$ and figure 9 for $g \to Q\bar{Q}(^1S_0^{[8]}) + X$, with $\mu_f = 2m_b$ and varying μ_r from m_b to $4m_b$. We find that, after NLO corrections, upper values of the error bands are larger than corresponding lower values of error bands by a factor of 2 in the middle z region. Using similar strategy, we find errors bands span by a factor of 3 in the charm quark case. The large theoretical uncertainties should be caused by the large NLO corrections. Yet we still do not fully understand the origination of large NLO corrections.

JHEP04(2019)116

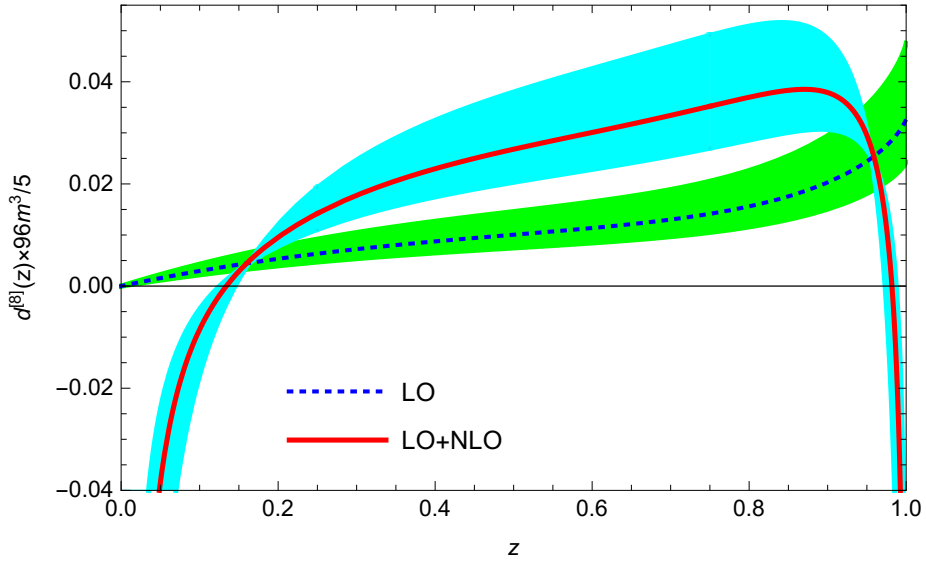

Figure 9. SDCs of the fragmentation function of $g \to b\bar{b}(^1S_0^{[8]}) + X$ at LO and NLO. The dotted line is for $d^{[8]}_{\rm LO}(z) \times (96m_b^3/5)$, while the solid line is for $\left(d^{[8]}_{\rm LO}(z) + d^{[8]}_{\rm NLO}(z)\right) \times (96m_b^3/5)$, with scale choices $\mu_r = \mu_f = 2m_b$. The bands are obtained by varying the renormalization scale μ_r by a factor of 2.

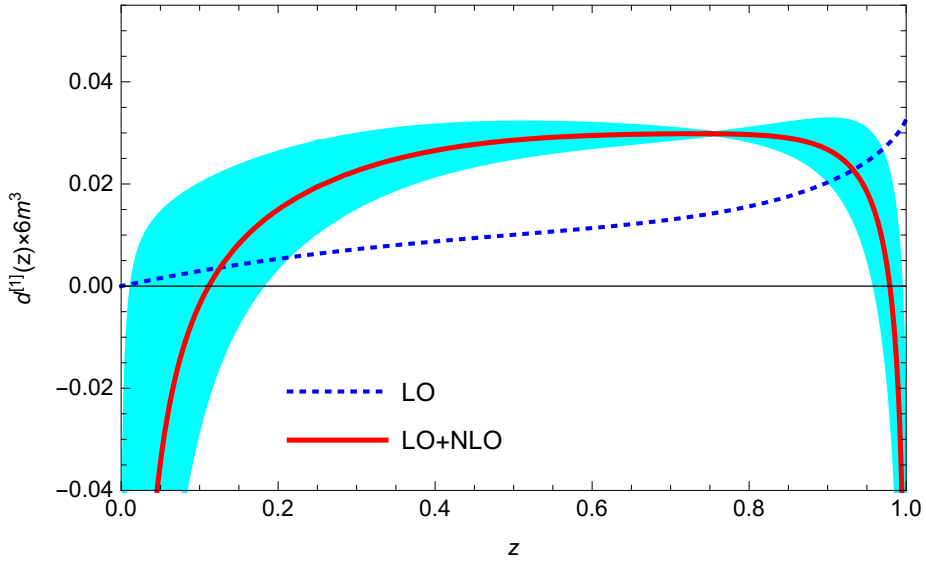

Figure 10. SDCs of the fragmentation function of $g \to b\bar{b}(^1S_0^{[1]}) + X$ at LO and NLO. The dotted line is for $d^{[1]}_{\rm LO}(z) \times (6m_b^3)$, while the solid line is for $\left(d^{[1]}_{\rm LO}(z) + d^{[1]}_{\rm NLO}(z)\right) \times (6m_b^3)$, with scale choices $\mu_r = \mu_f = 2m_b$. The bands are obtained by varying the renormalization scale μ_f by a factor of 2.

The sensitivities of LO and LO+NLO FFs with respect to the factorization scale μ_f are illustrated in figure 10 for $g \to Q\bar{Q}(^1S_0^{[1]}) + X$ and figure 11 for $g \to Q\bar{Q}(^1S_0^{[8]}) + X$, with $\mu_r = 2m_b$ and μ_f varying from m_b to $4m_b$. Note that the μ_f dependences should not be thought as theoretical uncertainties, because FFs are always defined at a specific value of μ_f.

JHEP04(2019)116

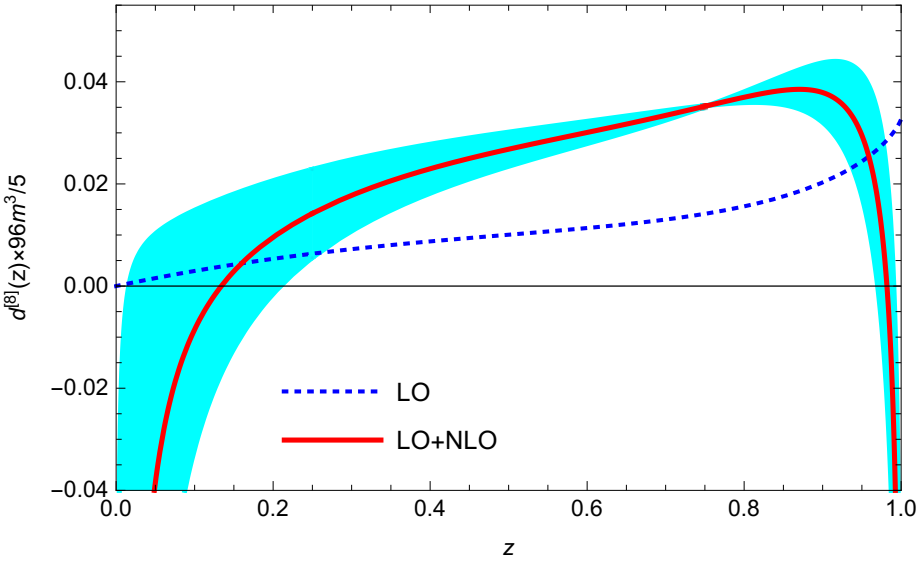

Figure 11. SDCs of the fragmentation function of $g \to b\bar{b}(^1S_0^{[8]}) + X$ at LO and NLO. The dotted line is for $d^{[8]}_{\rm LO}(z) \times (96m_b^3/5)$, while the solid line is for $\left(d^{[8]}_{\rm LO}(z) + d^{[8]}_{\rm NLO}(z)\right) \times (96m_b^3/5)$, with scale choices $\mu_r = \mu_f = 2m_b$. The bands are obtained by varying the renormalization scale μ_f by a factor of 2.

A IBP reduction with unregularized rapidity divergence

If all integrals are well regularized by dimensional regularization, IBP reduction relations should be independent of the infinitesimal imaginary parts $i\eta$, which means that coefficients of the relations are the same no matter a denominator is $E_j + i\eta$ or $E_j - i\eta$. This is the reason why we ignore the infinitesimal imaginary parts when using IBP reduction.

However, in this paper we encounter some integrals that can not be regularized by dimensional regularization only. There is a MI in the calculation of real correction

$$\int \mathrm{d}\Phi_{\rm real} \frac{1}{E_1\, E_4}\,, \tag{A.1}$$

which equals to

$$\frac{1}{(4\pi)^2 z^2}\int_0^1 \frac{\mathrm{d}z_1}{z_1}\int \frac{\mathrm{d}^{D-2}k_{1\perp}}{(2\pi)^{D-2}}\frac{\mathrm{d}^{D-2}k_{2\perp}}{(2\pi)^{D-2}}\frac{1}{(k_{2\perp}-k_{1\perp})^2\left(k_{1\perp}^2+\left(\frac{1-z}{z}\right)^2 z_1(1-z_1)+\frac{1-z}{z}(1-z_1)\right)}\,, \tag{A.2}$$

where we integrated out k_1^-, k_2^- and k_2^+, denoted $k_1^+ = (1-z)z_1 P_c^+$, and did the replacement

$$k_{1\perp} \to \sqrt{\frac{z_1}{1-z_1}}\, k_{1\perp}\,, \qquad k_{2\perp} \to \sqrt{\frac{1-z_1}{z_1}}\, k_{2\perp}\,. \tag{A.3}$$

It is clear now that the integration over z_1 is divergent at $z_1 = 0$ and it can not be regularized by dimensional regularization. This divergence is usually called rapidity divergence, and it is in fact well-known that it cannot be regularized by dimensional regularization. Similar problem exists when changing E_4 to E_5. Because the MI in eq. (A.1) is unregularized, on

JHEP04(2019)116

one hand we do not know how to calculate it, and on the other hand the IBP reduction which expresses SDCs as linear combination of MIs may give wrong result.

To explain why IBP reduction can be wrong, let us replace E_1, E_4 in eq. (3.2) respectively by

$$E_1' = (k_1 + k_2)^2, \qquad E_4' = (k_1 + P)^2, \tag{A.4}$$

which does not change the integral because of δ functions in the definition of $\mathrm{d}\Phi_{\mathrm{real}}$. If we then simply replace these δ functions by propagator denominators using eq. (3.3) and perform IBP reduction of original expression by ignoring the infinitesimal imaginary parts, we find two equal loop integrals,

$$\frac{P\cdot n}{z^2 2!}\int \frac{\mathrm{d}^D k_1}{(2\pi)^D}\frac{\mathrm{d}^D k_2}{(2\pi)^D}\frac{1}{E_1' E_4' E_{12} E_{13} E_{14}}\,, \tag{A.5}$$

and

$$\frac{1-2\epsilon}{\epsilon}\frac{(P\cdot n)^2}{z^2 2!}\int \frac{\mathrm{d}^D k_1}{(2\pi)^D}\frac{\mathrm{d}^D k_2}{(2\pi)^D}\frac{1}{E_1' E_4' E_8 E_{13} E_{14}}\,. \tag{A.6}$$

Because they are equal to each other, we can choose either the former or the later as our MI. However, on the other hand, once we replace propagator denominators back to δ functions, the eq. (A.6) will vanish as it lacks of E_{12}, while the eq. (A.5) will be changed to MI in eq. (A.1). Therefore, the final results are ambiguous.

To get unambiguous results both in the reduction step and in the calculation of MIs, we in principle need all involved integrals to be well regularized. We thus introduce an additional regulator besides spacetime dimension $D = 4 - 2\epsilon$, and take the limit of this new regulator to zero before take the limit of $\epsilon \to 0$. In this way, divergences that are regularized by dimensional regularization will not be affected. A possible choice of the new regulator is gluon mass in the phase space integration, which means we use

$$\mathrm{d}\Phi' = \frac{P\cdot n}{z^2 2!}\frac{\mathrm{d}^D k_1}{(2\pi)^{D-1}}\frac{\mathrm{d}^D k_2}{(2\pi)^{D-1}}\delta_+(k_1^2-m_g^2)\delta_+(k_2^2-m_g^2)\delta\left(k_1\cdot n + k_2\cdot n - \frac{1-z}{z}P\cdot n\right), \tag{A.7}$$

instead of $\mathrm{d}\Phi$. Note that, although gluon mass should also be introduced in Feynman amplitudes to be self-consistent, it is easy to show that only the gluon masses in phase space integration have non-vanishing effect. With this regulator, we find all involved integrals in our calculation are well regularized, and thus the IBP reduction do not introduce any ambiguity. After the IBP reduction and then take the limit $m_g \to 0$ in any place as far as the operation does not result in unregularized integrals, m_g still presents in four MIs

$$\int \mathrm{d}\Phi' \frac{1}{E_1\, E_4}\,, \qquad \int \mathrm{d}\Phi' \frac{1}{E_1\, E_4^2}\,, \qquad \int \mathrm{d}\Phi' \frac{P\cdot n}{E_1\, E_4\, E_9}\,, \qquad \int \mathrm{d}\Phi' \frac{P\cdot n}{E_1\, E_4\, E_{10}}\,, \tag{A.8}$$

besides the other four MIs obtained by changing E_4 to E_5.

As an example, we calculate the first MI in eq. (A.8) in the limit of $m_g \to 0$. After we integrate out k_1^-, k_2^-, k_2^+, $k_{2\perp}$ and $k_{1\perp}$ sequentially, we get

$$m_g^{-2\epsilon}\Gamma(\epsilon)^2 z^{-2}\int_0^1 \mathrm{d}z_1\, z_1^{-1+\epsilon}(1-2z_1+2z_1^2)^{-\epsilon}(t^2 z_1 + t + m_g^2/z_1)^{-\epsilon}, \tag{A.9}$$

JHEP04(2019)116

where $t = (1-z)/z$. Because of dimensional regularization, only the region $z_1 \sim m_g^2$ survives in the limit of $m_g \to 0$. So we set $z_1 = m_g^2\, y$ and take limit of $m_g \to 0$, then we get

$$\Gamma(\epsilon)^2 z^{-2} \int_0^\infty \mathrm{d}y\, y^{-1+\epsilon}(t+1/y)^{-\epsilon} = z^{-2+2\epsilon}(1-z)^{-2\epsilon}\Gamma(2\epsilon)\Gamma(\epsilon)\Gamma(-\epsilon)\,. \tag{A.10}$$

It tells us that, after introducing and then removing the gluon mass regulator, the MI in eq. (A.1) is eventually well regularized by dimensional regularization. We can similarly calculate the other three MIs in eq. (A.8), and find that they can be obtained from the first MI by multiplying factors $2\epsilon\,, 1$ and $z/(1-z)$, respectively.

Before describing how to apply the above method to our problem, let us first examine the following integral

$$\int \mathrm{d}\Phi \frac{1}{E_1 E_4 E_7}\,, \tag{A.11}$$

which is well regularized by dimensional regularization,[3] and thus we can calculate it numerically without introducing any other regulator. On the other hand, again without introducing any other regulator, we use IBP naively to reduce it to MIs. We find the reduced result is unique. All MIs obtained here except the one in eq. (A.1) are well regularized by dimensional regularization, which can be easily evaluated. Then if we replace the unregularized MI by eq. (A.10), we find the numerical result of eq. (A.11) agrees with the value calculated by applying IBP reduction. This test tells us two things. The first is that our gluon mass regulator can indeed give correct result. We thus take eq. (A.10) as the value of MIs defined in eq. (A.1), and similarly for other unregularized MIs. The second is that, if the original express is well regularized by dimensional regularization, using IBP naively may have no problem.

Based on the above lessons, we divide our original express two parts. The first part is well regularized by dimensional regularization, which is then reduced to MIs by using IBP naively. We check this part numerically and find good agreement between results before and after the IBP reduction. As the second part is unregularized, we introduce the above gluon mass regulator before applying IBP. After inserting the values of MIs, we find the second part in our decomposition eventually vanishes.

B Removable singularities and their effects

In this work, we encounter some removable singularities. Some of them determine the convergence radius of asymptotic expansion at some points, and others only decrease the precision of higher order coefficients in the asymptotic expansion. In the following discussion, to be definite we discuss the case where there is a removable singularity at $z = 1/2$ and there is a non-removable singularity at $z = 1$. We will do asymptotic expansion at $z = 0$.

Let us first discuss the case where there are more than one analytical structure at $z = 0$, and the singularity at $z = 1/2$ is removable only after the summation of contributions from

[3] It is well-regularized only if we first integrate out transverse momentum before integrate "+" momentum.

JHEP04(2019)116

all structures. Here is an example,

$$f(z) = \frac{\frac{\ln z}{1-z} + 2\ln 2}{1-2z}\,, \tag{B.1}$$

where $z = 1/2$ is indeed a removable singularity. When we do the asymptotic expansion at $z = 0$, we get two series, where one comes from the analytical part and the other one comes from the part proportional to $\ln z$. As $z = 1/2$ is a non-removable singularity of each of the two parts, the convergence radius of each of the series is $1/2$. Although $z = 1/2$ becomes a removable singularity in the summation of two parts, the convergence radius of the asymptotic expansion at $z = 0$ is still $1/2$. The reason is that we have no way to reorganize the two series to a single series so that it is convergent everywhere in $1/2 < |z| < 1$. In our calculation, MIs in real corrections have this kind of removable singularity at $z = 1/2$, which determine convergence radius of asymptotic expansion at both $z = 0$ and $z = 1$.

Now let us discuss the case where $z = 1/2$ is a removable singularity for each non-vanishing analytical structure at $z = 0$. A special case is that there is only one non-vanishing analytical structure, for example

$$g(z) = \frac{2\ln(2-2z)}{1-2z}\,, \tag{B.2}$$

where $1/2$ is a removable singularity while 1 is a branch point. If we denote

$$g(z) = \sum_{n=0}^{\infty} a_n z^n, \tag{B.3}$$

we have

$$a_n = 2^{n+1}\ln 2 - \sum_{i=0}^{n-1} \frac{2^{i+1}}{n-i}\,, \tag{B.4}$$

based on which we can calculate the convergence radius: $\lim_{n\to\infty} \frac{a_n}{a_{n+1}} = 1$. We thus find that the singularity $z = 1/2$ does not affect the convergence radius at $z = 0$. However, we will show that this singularity has other effects. To this purpose, we note that $g(z)$ satisfies the following DE,

$$\left(\frac{1}{2} - z\right)\frac{\mathrm{d}g(z)}{\mathrm{d}z} = g(z) - \frac{1}{1-z}\,, \tag{B.5}$$

with initial condition $g(0) = a_0 = 2\ln 2$. The DE can generate the recursion relation

$$a_{n+1} = 2a_n - \frac{2}{n+1}\,, \tag{B.6}$$

which determines higher order coefficients in the expansion. However, when we solve DEs numerically, the initial condition can have only finite precision. If we denote the absolute error of a_0 as λ, the absolute error of a_n calculated from the recursion relation is $2^n\lambda$. At the point $z = x$, the contributed error from a_n is $(2x)^n\lambda$, which is much larger than λ if $x > 1/2$ and n is large. If we reduce this error by truncating the expansion to small n, then

there will be a large systematic error at the order of x^n. The best accuracy at $z = x$ that one can obtain is to choose a truncation n so that $(2x)^n\lambda \sim x^n$, which gives $n \sim \log_2 \lambda^{-1}$ and $x^n \sim \lambda^{-\log_2 x}$. For example, for the point $x = \sqrt{2}/2$, the smallest absolute error that we can get is $\lambda^{1/2}$, which is larger than the absolute error λ at $x = 0$.

In virtual corrections, if we do asymptotic expansion at $z = 1$, the removable singularity at $z = 2(\sqrt{2}-1)$ belongs to the second type, and the convergence radius is determined by the singularity at $z = 0$. Let us denote $1 - 2(\sqrt{2}-1) = a^{-1}$, then the best accuracy at $z = 1-x$ that we can obtained is determined by $(ax)^n\lambda \sim x^n$, which gives $n \sim \log_a \lambda^{-1}$ and $x^n \sim \lambda^{-\log_a x}$. In this work, we want to estimate the value at $z = 3/4$ from the expansion at $z = 1$, which gives the best accuracy about $\lambda^{0.786}$. If we need the accuracy to be about 10^{-15}, we find $\lambda \sim 10^{-19}$ and $n \sim 25$, which means that we need initial condition for the expansion at $z = 1$ to have four more significant digits.

C Boundary conditions of MIs in real corrections

MIs in real corrections have the form

$$\int \mathrm{d}\Phi_{\mathrm{real}} \frac{1}{E_a^{n_a} E_b^{n_b} E_c^{n_c} E_d^{n_d}}\,, \tag{C.1}$$

where $d \in \{8, 9, 10, 11\}$, $a, b, c \in \{1, \ldots, 7\}$ and $\mathrm{d}\Phi_{\mathrm{real}}$ is defined in eq. (3.1). We calculate most MIs in the limit $z \to 1$ in this appendix, with the other MIs which are not regularized by dimensional regularization calculated in appendix A. From eq. (3.1), $\delta\big(k_1 \cdot n + k_2 \cdot n - \frac{1-z}{z} P \cdot n\big)$ together with conditions $k_1^+ > 0$ and $k_2^+ > 0$ requires that k_1^+ and k_2^+ must be at the order of $1 - z$ when $z \to 1$. Otherwise, if taking $k_1^+ \ll (1-z)P^+$ as an example, the integral will be proportional to

$$\int_0^\infty \mathrm{d}k_1^+ \, (k_1^+)^{a+b\epsilon}, \tag{C.2}$$

which equals 0 in dimensional regularization. Introducing the parametrization $k_1^+ = (1-z)z_1P_c^+$ and $k_2^+ = (1-z)(1-z_1)P_c^+$, $\mathrm{d}\Phi_{\mathrm{real}}$ becomes

$$\int \mathrm{d}\Phi_{\mathrm{real}} = \frac{1}{(4\pi)^2 z(1-z)2!} \int_0^1 \frac{\mathrm{d}z_1}{z_1(1-z_1)} \int \frac{\mathrm{d}^{D-2}k_{1\perp}}{(2\pi)^{D-2}} \frac{\mathrm{d}^{D-2}k_{2\perp}}{(2\pi)^{D-2}}\,. \tag{C.3}$$

JHEP04(2019)116

In the limit of $z \to 1$, E_i given in eq. (3.2) become

$$\begin{aligned}
\hat{E}_1 &= \frac{1}{2}\left(\frac{1-z_1}{z_1}k_{1\perp}^2 + \frac{z_1}{1-z_1}k_{2\perp}^2 - 2k_{1\perp}\cdot k_{2\perp}\right), \\
\hat{E}_2 &= \frac{1}{2\lambda}\left(\frac{k_{1\perp}^2}{z_1} + \lambda^2 z_1\right), \\
\hat{E}_3 &= \frac{1}{2\lambda}\left(\frac{k_{2\perp}^2}{1-z_1} + \lambda^2(1-z_1)\right), \\
\hat{E}_4 &= \frac{1}{\lambda}\left(\frac{k_{1\perp}^2}{z_1} + \lambda\right), \\
\hat{E}_5 &= \frac{1}{\lambda}\left(\frac{k_{2\perp}^2}{1-z_1} + \lambda\right), \\
\hat{E}_6 &= \frac{1}{2\lambda}\left(\frac{k_{1\perp}^2}{z_1} + \frac{k_{2\perp}^2}{1-z_1} + \lambda^2\right), \\
\hat{E}_7 &= \frac{1}{\lambda}\left(\frac{k_{1\perp}^2}{z_1} + \frac{k_{2\perp}^2}{1-z_1} + \lambda\right),
\end{aligned} \tag{C.4}$$

where $\lambda = 1 - z$. As $\lambda \to 0$, each MI has at most four non-vanishing regions,

$$\begin{aligned}
&k_{1\perp}^2 \sim \lambda^2, && k_{2\perp}^2 \sim \lambda^2\,; \\
&k_{1\perp}^2 \sim \lambda^2, && k_{2\perp}^2 \sim \lambda\,; \\
&k_{1\perp}^2 \sim \lambda\,, && k_{2\perp}^2 \sim \lambda^2\,; \\
&k_{1\perp}^2 \sim \lambda\,, && k_{2\perp}^2 \sim \lambda\,.
\end{aligned} \tag{C.5}$$

To obtain boundary conditions, we only need to calculate the leading contribution in each region, which is proportional to $\lambda^{n\epsilon}$ with $n = -2, -3$ or -4. The calculation is a little different depending on whether E_1 presents in eq. (C.1).

Without E_1, there is no cross term $k_{1\perp}\cdot k_{2\perp}$ in the limit $\lambda \to 0$. We thus first rescale momenta by

$$k_{1\perp} \to \sqrt{z_1}\, k_{1\perp}\,, \qquad k_{2\perp} \to \sqrt{1-z_1}\, k_{2\perp}\,, \tag{C.6}$$

and then integrate out $k_{2\perp}$. After that, the integration over $k_{1\perp}$ is very simple unless it has the form

$$\int \frac{\mathrm{d}^{D-2}k_{1\perp}}{(2\pi)^{D-2}} \frac{1}{(k_{1\perp}^2+1)^{n_1}\left(k_{1\perp}^2 + a(z_1)\right)^{n_2}}\,, \tag{C.7}$$

with $a(z_1) \neq 0, 1$. For this kind of integrals, we integrated out $k_{1\perp}$ after Feynman parametrization. Finally, the integration over z_1 and Feynman parameters can be calculated analytically with the help of sector decomposition refs. [80, 81], which can isolate mixed divergences from parameter integrals. There are two widely used programs that can do the sector decomposition, SecDec [82–85] and FIESTA [86–89]. We use SecDec in this paper.

If E_1 presents, we first rescale momenta by

$$k_{1\perp} \to \sqrt{\frac{z_1}{1-z_1}}\, k_{1\perp}\,, \qquad k_{2\perp} \to \sqrt{\frac{1-z_1}{z_1}}\, k_{2\perp}\,, \tag{C.8}$$

JHEP04(2019)116

and then do the the replacement $k_{1\perp} \to k_{1\perp} + k_{2\perp}$, which changes $\hat{E}_1$ to $k_{1\perp}^2$ and moves the cross term $k_{1\perp}\cdot k_{2\perp}$ to other denominators. To proceed, we introduce Feynman parametrization and integrate out $k_{2\perp}$. Then the integration of $k_{1\perp}$ has the form

$$\int \frac{\mathrm{d}^{D-2}k_{1\perp}}{(2\pi)^{D-2}} \frac{1}{(k_{1\perp}^2)^{n_1}\left(k_{1\perp}^2 + a(z_1)\right)^{n_2}}\,, \tag{C.9}$$

which can be easily integrated out. Finally, integration of Feynman parameters can be worked out with the help of sector decomposition.

All analytical results of MIs calculated here have been checked by numerical results computed by SecDec, and good agreement is found.

D Calculation of MIs in virtual corrections

MIs for virtual corrections in eq. (4.1) can be expressed as

$$\frac{1}{4\pi z(1-z)} \int \frac{\mathrm{d}^{D-2}k_\perp}{(2\pi)^{D-2}} \frac{\mathrm{d}^D l}{(2\pi)^D} \prod_i \frac{1}{F_i^{\nu_i}}\,, \tag{D.1}$$

where F_i are defined in eq. (4.2) with $k^2 = 0$, $k^- = k_\perp^2/(2k^+)$ and $k^+ = (1-z)P^+/z$. We apply the method proposed in refs. [75, 76] to calculate these MIs at any regular point $z = z_0$. To this purpose, we change F_i to $F_i + i\eta$ for $i \neq 1, 2$ to obtain new MIs. We can set up DEs of the new MIs by first differentiating them with respect to η and then reducing the obtained expressions to the new MIs using IBP reduction. If we also know boundary conditions of the new MIs at a special value of η, we can solve the DEs numerically to obtain the new MIs at $\eta = 0^+$ with very high precision, which are nothing but our desired old MIs.

The boundary that we choose is at $\eta \to \infty$. To calculate the boundary conditions, we first perform Feynman parameterization and then shift l to remove cross terms. The obtained results are proportional to

$$\iint \mathrm{d}x_1 \ldots \mathrm{d}x_n \int \frac{\mathrm{d}^{D-2}k_\perp}{(2\pi)^{D-2}} \frac{\mathrm{d}^D l}{(2\pi)^D} \frac{1}{(k_\perp^2 + a)^{n_1}(l^2 - b\,k_\perp^2 - c + i\eta)^{n_2}\,(l\cdot n + d + i\eta)^{n_3}}\,, \tag{D.2}$$

where b, c, d are functions of z and the Feynman parameters $x_1, \ldots, x_n$, and a is a function of z. As $\eta \to \infty$, there are only two regions for this integral,

$$\begin{aligned} l^2 &\sim \eta\,, \qquad & k_\perp^2 &\sim 1\,; \\ l^2 &\sim \eta\,, \qquad & k_\perp^2 &\sim \eta\,. \end{aligned} \tag{D.3}$$

The leading term of the first region gives

$$\eta^{2-n_2-n_3-\epsilon}\, i^{-n_3} \iint \mathrm{d}x_1 \ldots \mathrm{d}x_n \int \frac{\mathrm{d}^{D-2}k_\perp}{(2\pi)^{D-2}} \frac{1}{(k_\perp^2 + a)^{n_1}} \int \frac{\mathrm{d}^D l}{(2\pi)^D} \frac{1}{(l^2 + i)^{n_2}}\,, \tag{D.4}$$

which can be easily integrated out. The leading term of the second region gives

$$\eta^{3-n_1-n_2-n_3-2\epsilon}\, i^{-n_3} \iint \mathrm{d}x_1 \ldots \mathrm{d}x_n \int \frac{\mathrm{d}^{D-2}k_\perp}{(2\pi)^{D-2}} \frac{1}{(k_\perp^2)^{n_1}} \int \frac{\mathrm{d}^D l}{(2\pi)^D} \frac{1}{(l^2 - b\,k_\perp^2 + i)^{n_2}}\,, \tag{D.5}$$

JHEP04(2019)116

the integrand of which is proportional to $b^{n_1-1+\epsilon}$ after integrating out $k_\perp$ and l. Though b is a function of Feynman parameters and z, the dependence of z can be factorized out. So the integration over Feynman parameters can be easily performed.

E Coefficients

In this appendix, we give the coefficients defined in eq. (6.3). The coefficients of asymptotic expansion at $z = 0$ with different powers of $\ln(z)$ are shown respectively in tables 3–5. The coefficients of asymptotic expansion at $z = 1/2$ are shown in table 6. The coefficients of asymptotic expansion at $z = 1$ with different powers of $\ln(1 - z)$ are shown respectively in tables 7–10. To obtain results with 160-digit precision at any value of z, we attach an ancillary file with these coefficients calculated up to $j = 530$.

Acknowledgments

We thank Hao-Yu Liu and Yu-Jie Zhang for useful discussions, and thank Feng Feng and Yu Jia for useful communications. The work is supported in part by the National Natural Science Foundation of China (Grants No. 11475005 and No. 11075002), the National Key Basic Research Program of China (No. 2015CB856700), and High-performance Computing Platform of Peking University.

Note added. While this paper was being finalized, two related preprints appeared [90, 91]. In ref. [90], the authors calculated NLO corrections for FF of $g \to Q\bar{Q}(^1S_0^{[8]}) + X$ using FKS subtraction method; while in ref. [91], the authors calculated NLO corrections for FFs of $g \to Q\bar{Q}(^1S_0^{[1]}) + X$ and $g \to Q\bar{Q}(^1S_0^{[8]}) + X$ using sector decomposition. Our high-precision results agree with K-factors obtained in these two works within their estimated errors.

JHEP04(2019)116

j	$2^j\, A^f_{2j}$	$2^j\, A^N_{2j}$	$A^{[1]}_{2j}$	$A^{[8]}_{2j}$
0	0	0	0	0
1	0	0	−0.12500000000000	−0.50000000000000
2	0	0.062500000000000	0.17187500000000	0.18750000000000
3	0	0	0.40625000000000	0.43750000000000
4	0	0.010416666666667	0.41992187500000	0.58333333333333
5	0	0.012500000000000	0.61302083333333	0.83072916666667
6	0	0.012500000000000	0.77320963541667	1.0865885416667
7	0	0.011904761904762	0.96474144345238	1.3835937500000
8	0	0.011160714285714	1.1624375116257	1.7071149553571
9	0	0.010416666666667	1.3765091668992	2.0620698474702
10	0	0.0097222222222222	1.6032713269430	2.4461819118924
11	0	0.0090909090909091	1.8448080307822	2.8605321490575
12	0	0.0085227272727273	2.1006452758591	3.3048841336073
13	0	0.0080128205128205	2.3713380017388	3.7796014959162
14	0	0.0075549450549451	2.6569079570824	4.2847597683451
15	0	0.0071428571428571	2.9575555837436	4.8205296219487
16	0	0.0067708333333333	3.2733526663303	5.3870027269636
17	0	0.0064338235294118	3.6043937236582	5.9842752947952
18	0	0.0061274509803922	3.9507353541372	6.6124149853725
19	0	0.0058479532163743	4.3124309604004	7.2714813347533
20	0	0.0055921052631579	4.6895195736275	7.9615206143639
21	0	0.0053571428571429	5.0820347557021	8.6825717844530
22	0	0.0051406926406926	5.4900031588248	9.4346665064663
23	0	0.0049407114624506	5.9134472546027	10.217831334440
24	0	0.0047554347826087	6.3523855949021	11.032088390171
25	0	0.0045833333333333	6.8068338723260	11.877456377491
26	0	0.0044230769230769	7.2768053293128	12.753951144117
27	0	0.0042735042735043	7.7623112742042	13.661586235331
28	0	0.0041335978835979	8.2633613935222	14.600373279871
29	0	0.0040024630541872	8.7799640454746	15.570322323673
30	0	0.0038793103448276	9.3121264733205	16.571442086004
31	0	0.0037634408602151	9.8598549881702	17.603740172815
32	0	0.0036542338709677	10.423155112584	18.667223247831
33	0	0.0035511363636364	11.002031700614	19.761897174325
34	0	0.0034536541889483	11.596489035538	20.887767131486
35	0	0.0033613445378151	12.206530911465	22.044837711381
36	0	0.0032738095238095	12.832160701094	23.233112999755
37	0	0.0031906906906907	13.473381412637	24.452596643923
38	0	0.0031116642958748	14.130195737711	25.703291909998
39	0	0.0030364372469636	14.802606091904	26.985201731406
40	0	0.0029647435897436	15.490614649253	28.298328750170

Table 3. Coefficients of the term including $\ln^2(z)$ in the asymptotic expansion at $z = 0$.

JHEP04(2019)116

j	$2^j\, A^f_{1j}$	$2^j\, A^N_{1j}$	$A^{[1]}_{1j}$	$A^{[8]}_{1j}$
0	0	0	0	0
1	−0.50000000000000	0.40342640972003	0.57398486804019	2.1705584583202
2	0.50000000000000	−0.56250000000000	1.4045473411516	1.5117808350766
3	−0.16666666666667	0.22822546990668	0.93487513830781	0.99773602488115
4	−0.083333333333333	0.063728942128898	0.77583977358195	1.1446460363136
5	−0.050000000000000	0.022603443749342	1.2365719430589	1.6550348228586
6	−0.033333333333333	0.0083258186336740	1.4092448914801	2.0468490402404
7	−0.023809523809524	0.0026716127522174	1.7361186602102	2.5406880555688
8	−0.017857142857143	0.00032676908567975	2.0196361310846	3.0423344345641
9	−0.013888888888889	−0.00063076082765445	2.3512179222451	3.5982593417265
10	−0.011111111111111	−0.00098315445723759	2.6900249599261	4.1889435565027
11	−0.0090909090909091	−0.0010700359072207	3.0552572573464	4.8243295123460
12	−0.0075757575757576	−0.0010438451264836	3.4384052244977	5.5004264496101
13	−0.0064102564102564	−0.00097377622797185	3.8437040732642	6.2195037543678
14	−0.0054945054945055	−0.00089095569474677	4.2693965297393	6.9807979692039
15	−0.0047619047619048	−0.00080888658331143	4.7164846138369	7.7848921322315
16	−0.0041666666666667	−0.00073292167756481	5.1846360515956	8.6316844605753
17	−0.0036764705882353	−0.00066470610592851	5.6741210281724	9.5213601185356
18	−0.0032679738562092	−0.00060426584550321	6.1849023934097	10.453940889020
19	−0.0029239766081871	−0.00055098207513755	6.7170723197927	11.429505551778
20	−0.0026315789473684	−0.00050403611185787	7.2706479877643	12.448089618283
21	−0.0023809523809524	−0.00046260357211663	7.8456719124648	13.509736676690
22	−0.0021645021645022	−0.00042593116202551	8.4421660426331	14.614476407438
23	−0.0019762845849802	−0.00039335992204217	9.0601554299886	15.762337114500
24	−0.0018115942028986	−0.00036432525363425	9.6996581355889	16.953341233177
25	−0.0016666666666667	−0.00033834791659660	10.360691100613	18.187508691798
26	−0.0015384615384615	−0.00031502244008527	11.043268112937	19.464856235503
27	−0.0014245014245014	−0.00029400570927271	11.747401426065	20.785398505998
28	−0.0013227513227513	−0.00027500677270258	12.473101486693	22.149148123601
29	−0.0012315270935961	−0.00025777814198227	13.220377479519	23.556116136380
30	−0.0011494252873563	−0.00024210852946522	13.989237398849	25.006312200449
31	−0.0010752688172043	−0.00022781685111583	14.779688288806	26.499744818788
32	−0.0010080645161290	−0.00021474729572681	15.591736353070	28.036421494339
33	−0.00094696969696970	−0.00020276527369408	16.425387089137	29.616348878805
34	−0.00089126559714795	−0.00019175408363014	17.280645379247	31.239532886426
35	−0.00084033613445378	−0.00018161216223762	18.157515576954	32.905978794662
36	−0.00079365079365079	−0.00017225080769429	19.056001575036	34.615691326624
37	−0.00075075075075075	−0.00016359228794356	19.976106865459	36.368674722171
38	−0.00071123755334282	−0.00015556826266034	20.917834589155	38.164932797826
39	−0.00067476383265857	−0.00014811846167822	21.881187579114	40.004468998286
40	−0.00064102564102564	−0.00014118957386764	22.866168397045	41.887286440479

Table 4. Coefficients of the term including $\ln^1(z)$ in the asymptotic expansion at $z = 0$.

JHEP04(2019)116

j	$2^j\, A^f_{0j}$	$2^j\, A^N_{0j}$	$A^{[1]}_{0j}$	$A^{[8]}_{0j}$
0	0	0	3.4252812215960	3.4252812215960
1	−0.70456854629337	1.4697992278829	4.6689187537857	6.1685539364111
2	0.25000000000000	−1.1843929628919	−1.8640969877500	−2.8881394426089
3	0.17298364660445	0.094965152253727	−0.16554393253699	0.51213384853759
4	−0.045452621142219	0.23072894840510	0.78382242411568	0.85936906668774
5	−0.066577128240887	0.17053547870878	0.44336647144137	0.73994308173799
6	−0.063366233642073	0.12109747519709	0.67331915427375	0.96405497622222
7	−0.056542774596945	0.087614056243353	0.72643591336692	1.1148648188725
8	−0.049872358725487	0.065138970095316	0.86374734795843	1.3236172730145
9	−0.044061671976084	0.049781093512754	0.97691299177752	1.5305055344041
10	−0.039144013506793	0.039034884002099	1.1101510178493	1.7590775589338
11	−0.035004464286014	0.031325828249495	1.2448043644419	1.9991406479620
12	−0.031510629609838	0.025657937682758	1.3891309165733	2.2552261847826
13	−0.028545040478971	0.021391957753787	1.5396189149342	2.5254422703430
14	−0.026010792203882	0.018110414250278	1.6979242952360	2.8107253874451
15	−0.023829906843410	0.015535501281597	1.8633587742894	3.1107172815180
16	−0.021940102001844	0.013478693328440	2.0362782983433	3.4256301152076
17	−0.020291630604230	0.011809471062524	2.2165508569299	3.7554031028881
18	−0.018844617116018	0.010435658435772	2.4042617391595	4.1000931093606
19	−0.017566929679332	0.0092908842985695	2.5993906536078	4.4596966727796
20	−0.016432517354084	0.0083264647109326	2.8019628414668	4.8342342183080
21	−0.015420121785057	0.0075060622043309	3.0119795344474	5.2237117778890
22	−0.014512280853376	0.0068021129583808	3.2294511242571	5.6281396460192
23	−0.013694556865817	0.0061933957846504	3.4543820046562	6.0475241093669
24	−0.012954936500540	0.0056633497945082	3.6867780428773	6.4818717308353
25	−0.012283362047158	0.0051988907233773	3.9266432894214	6.9311876101839
26	−0.011671363211814	0.0047895646955148	4.1739817310093	7.3954764370257
27	−0.011111766227744	0.0044269339720905	4.4287966091054	7.8747421701539
28	−0.010598462663998	0.0041041246704996	4.6910908677894	8.3689883364117
29	−0.010126224574093	0.0038154892744314	4.9608670398859	8.8782180067257
30	−0.0096905558141942	0.0035563516646064	5.2381273837575	9.4024339054297
31	−0.0092875717533919	0.0033228122754372	5.5228738857788	9.9416384388550
32	−0.0089139013993049	0.0031115976166264	5.8151083158355	10.495833749157
33	−0.0085666073218522	0.0029199429178158	6.1148322480858	11.065021745042
34	−0.0082431197889759	0.0027454997753454	6.4220470909011	11.649204134677
35	−0.0079411823135248	0.0025862628642111	6.7367541061961	12.248382450199
36	−0.0076588064118678	0.0024405113261225	7.0589544287767	12.862558070213
37	−0.0073942338376384	0.0023067615547164	7.3886490814482	13.491732238224
38	−0.0071459049121013	0.0021837289043051	7.7258389886494	14.135906078845
39	−0.0069124318511479	0.0020702964389732	8.0705249878506	14.795080611558
40	−0.0066925762066937	0.0019654892760815	8.4227078395553	15.469256762702

Table 5. Coefficients of the term including $\ln^0(z)$ in the asymptotic expansion at $z = 0$.

JHEP04(2019)116

j	B_j^f	B_j^N	$B_j^{[1]}$	$B_j^{[8]}$
0	−0.16851770326295	0.41612862149279	3.4502975889603	3.1359899450428
1	−0.28278529964508	0.35334086558632	0.42316029178587	2.2549071617698
2	0.033232765296908	−0.078926461470642	−2.4479134932754	−1.2096826020440
3	−0.020468226170618	0.18257241446333	1.3806416076688	1.5894441359737
4	−0.14037814600712	0.18764848019285	−1.3100405280826	−1.0254411711450
5	−0.065776956191377	0.074435996336763	0.39126631701522	0.25474714881661
6	−0.076860753906582	0.068406036987869	−1.5646863364829	−1.5566491831871
7	−0.046950966357598	0.033611273229861	0.40381458231355	0.21319989582011
8	−0.050729242941967	0.034248119325764	−1.5303231186726	−1.6118306150112
9	−0.034864417756233	0.018849286758299	0.47363972162014	0.28152365204275
10	−0.036914263377718	0.020548082773928	−1.4706719667535	−1.5832992441957
11	−0.027191811319423	0.012105804040568	0.53859653194338	0.35621228190425
12	−0.028565671912742	0.013735845824808	−1.4169118860031	−1.5396619168110
13	−0.022043774469329	0.0084582196164943	0.59223102386109	0.42155640308020
14	−0.023064062765382	0.0098442114801508	−1.3722504391114	−1.4966631611278
15	−0.018406627098339	0.0062522624645907	0.63575099421848	0.47636585731335
16	−0.019207900828926	0.0074059596217084	−1.3355336251243	−1.4579860431543
17	−0.015725574144345	0.0048127407975187	0.67127156389260	0.52214798327752
18	−0.016377071313228	0.0057753762958888	−1.3051503967425	−1.4240860212676
19	−0.013680301725950	0.0038201885977304	0.70061447318763	0.56064719921929
20	−0.014222889561732	0.0046305266387179	−1.2797303934160	−1.3945398884440
21	−0.012075838152948	0.0031064803097827	0.72517425732263	0.59334093028222
22	−0.012535906633085	0.0037956652982329	−1.2582129267355	−1.3687399929482
23	−0.010787850505734	0.0025759385521478	0.74598991589784	0.62139093121312
24	−0.011183512355657	0.0031680450206490	−1.2397948295255	−1.3461030762910
25	−0.0097338247794586	0.0021707493510462	0.76383548086394	0.64569354140257
26	−0.010078064196233	0.0026842711508940	−1.2238677415693	−1.3261252483808
27	−0.0088571028090975	0.0018542686601597	0.77929301723785	0.66694014586286
28	−0.0091595360435268	0.0023034840146319	−1.2099669946673	−1.3083872688362
29	−0.0081176272567437	0.0016023432021528	0.79280579496772	0.68566776608843
30	−0.0083855603387736	0.0019983773878152	−1.1977336654198	−1.2925449365197
31	−0.0074863542106615	0.0013985224518692	0.80471594074944	0.70229760367572
32	−0.0077254540444392	0.0017501362421637	−1.1868871664174	−1.2783164432622
33	−0.0069417578505870	0.0012312853690261	0.81529101005047	0.71716353672909
34	−0.0071564964635966	0.0015454523692259	−1.1772055371491	−1.2654705594653
35	−0.0064675743925251	0.0010923669606980	0.82474286322051	0.73053304052605
36	−0.0066615331494768	0.0013746965638203	−1.1685112004789	−1.2538166822664
37	−0.0060513051734458	0.00097571253275151	0.83324121877091	0.74262258886253
38	−0.0062273889483643	0.0012307617616398	−1.1606605749105	−1.2431967939952
39	−0.0056831988213171	0.00087680407439360	0.84092350493513	0.75360907400686
40	−0.0058437903118448	0.0011083095732526	−1.1535364167066	−1.2334790765198

Table 6. Coefficients of the asymptotic expansion at $z = 1/2$.

JHEP04(2019)116

j	$2^j\, C_{3j}^f$	$2^j\, C_{3j}^N$	$C_{3j}^{[1]}$	$C_{3j}^{[8]}$
0	0	0	0	0
1	0	0	−0.83333333333333	−1.0000000000000
2	0	0	0.12500000000000	0.062500000000000
3	0	0	0	0
4	0	0	0	0
5	0	0	0	0
6	0	0	0	0
7	0	0	0	0
8	0	0	0	0
9	0	0	0	0
10	0	0	0	0
11	0	0	0	0
12	0	0	0	0
13	0	0	0	0
14	0	0	0	0
15	0	0	0	0
16	0	0	0	0
17	0	0	0	0
18	0	0	0	0
19	0	0	0	0
20	0	0	0	0
21	0	0	0	0
22	0	0	0	0
23	0	0	0	0
24	0	0	0	0
25	0	0	0	0
26	0	0	0	0
27	0	0	0	0
28	0	0	0	0
29	0	0	0	0
30	0	0	0	0
31	0	0	0	0
32	0	0	0	0
33	0	0	0	0
34	0	0	0	0
35	0	0	0	0
36	0	0	0	0
37	0	0	0	0
38	0	0	0	0
39	0	0	0	0
40	0	0	0	0

Table 7. Coefficients of the term including $\ln^3(1-z)$ in the asymptotic expansion at $z = 1$.

JHEP04(2019)116

j	$2^j\, C_{2j}^f$	$2^j\, C_{2j}^N$	$C_{2j}^{[1]}$	$C_{2j}^{[8]}$
0	0	0	−0.50000000000000	−1.0000000000000
1	0.50000000000000	0	0.37500000000000	0.12500000000000
2	0	0	0.50000000000000	0.15625000000000
3	0	0	−0.60416666666667	−0.87500000000000
4	0	0	−0.34635416666667	−0.72135416666667
5	0	0	−0.35052083333333	−0.83411458333333
6	0	0	−0.38502604166667	−0.97376302083333
7	0	0	−0.43921130952381	−1.1611421130952
8	0	0	−0.51572265625000	−1.3897426060268
9	0	0	−0.61328900049603	−1.6551300533234
10	0	0	−0.72943289620536	−1.9555071149554
11	0	0	−0.86277792574179	−2.2895857465560
12	0	0	−1.0130357310197	−2.6566851969577
13	0	0	−1.1799183499470	−3.0563270136100
14	0	0	−1.3631643781600	−3.4882098354713
15	0	0	−1.5625995583057	−3.9521164788987
16	0	0	−1.7781207862923	−4.4478939551494
17	0	0	−2.0096467849050	−4.9754273064916
18	0	0	−2.2571121633958	−5.5346296712624
19	0	0	−2.5204664136241	−6.1254332211172
20	0	0	−2.7996704241174	−6.7477843824523
21	0	0	−3.0946924018735	−7.4016400405593
22	0	0	−3.4055061873651	−8.0869651205236
23	0	0	−3.7320901937905	−8.8037307378166
24	0	0	−4.0744264633797	−9.5519128887260
25	0	0	−4.4324998780102	−10.331491446636
26	0	0	−4.8062976159231	−11.142449408254
27	0	0	−5.1958087389786	−11.984772306809
28	0	0	−5.6010238595632	−12.858447755577
29	0	0	−6.0219348723453	−13.763465086182
30	0	0	−6.4585347425683	−14.699815060482
31	0	0	−6.9108173355185	−15.667489638499
32	0	0	−7.3787772771983	−16.666481790253
33	0	0	−7.8624098399109	−17.696785341976
34	0	0	−8.3617108480247	−18.758394849621
35	0	0	−8.8766765997782	−19.851305494155
36	0	0	−9.4073038019765	−20.975512994373
37	0	0	−9.9535895151783	−22.131013533921
38	0	0	−10.515531107478	−23.317803699878
39	0	0	−11.093126215343	−24.535880430829
40	0	0	−11.686372710287	−25.785240972751

Table 8. Coefficients of the term including $\ln^2(1-z)$ in the asymptotic expansion at $z = 1$.

JHEP04(2019)116

j	$2^j\, C_{1j}^f$	$2^j\, C_{1j}^N$	$C_{1j}^{[1]}$	$C_{1j}^{[8]}$
0	0.16666666666667	0	0.37320146702979	−1.2717325998184
1	−0.83333333333333	3.0000000000000	1.2317374615085	5.1665396620531
2	−1.3333333333333	−1.0000000000000	−0.0049415864371726	−0.72501733141193
3	0	1.7777777777778	−0.39583333333333	−1.2048611111111
4	0	−1.1666666666667	−0.27777777777778	−0.94843750000000
5	0	1.1733333333333	−0.55451388888889	−1.4184027777778
6	0	−1.0666666666667	−0.58496961805556	−1.6571884300595
7	0	1.0775510204082	−0.76076140873016	−2.0457971053005
8	0	−1.0357142857143	−0.89078802061189	−2.4197029982240
9	0	1.0440917107584	−1.0690909387844	−2.8659408280999
10	0	−1.0222222222222	−1.2604599181252	−3.3457155692993
11	0	1.0284664830119	−1.4812527410936	−3.8767821276542
12	0	−1.0151515151515	−1.7217815999456	−4.4498991482114
13	0	1.0199031737493	−1.9862444565446	−5.0689360493821
14	0	−1.0109890109890	−2.2724855553188	−5.7315689661375
15	0	1.0147008547009	−2.5813070161657	−6.4386168752643
16	0	−1.0083333333333	−2.9120850939700	−7.1894448486906
17	0	1.0113033448674	−3.2649946515199	−7.9841914861373
18	0	−1.0065359477124	−3.6398583480110	−8.8226548755166
19	0	1.0089620335669	−4.0366845785431	−9.7048301626652
20	0	−1.0052631578947	−4.4554039346054	−10.630636010721
21	0	1.0072801050245	−4.8959997271497	−11.600044668106
22	0	−1.0043290043290	−5.3584385359755	−12.613013813211
23	0	1.0060311459177	−5.8427017364928	−13.669517729188
24	0	−1.0036231884058	−6.3487688117350	−14.769529890133
25	0	1.0050782608696	−6.8766247677079	−15.913030161841
26	0	−1.0030769230769	−7.4262555253483	−17.100000108663
27	0	1.0043347050754	−7.9976495249565	−18.330424461170
28	0	−1.0026455026455	−8.5907964418184	−19.604289700477
29	0	1.0037433390584	−9.2056874302096	−20.921584215344
30	0	−1.0022988505747	−9.8423146685881	−22.282297781623
31	0	1.0032652768309	−10.500671315910	−23.686421461447
32	0	−1.0020161290323	−11.180751314226	−25.133947357953
33	0	1.0028733078586	−11.882549305241	−26.624868493459
34	0	−1.0017825311943	−12.606060519716	−28.159178667350
35	0	1.0025479282622	−13.351280705239	−29.736872357411
36	0	−1.0015873015873	−14.118206055173	−31.357944626608
37	0	1.0022748617343	−14.906833153491	−33.022391049349
38	0	−1.0014224751067	−15.717158925268	−34.730207646287
39	0	1.0020434635819	−16.549180595653	−36.481390829981
40	0	−1.0012820512821	−17.402895654033	−38.275937357712

Table 9. Coefficients of the term including $\ln^1(1-z)$ in the asymptotic expansion at $z = 1$.

JHEP04(2019)116

j	$2^j\, C_{0j}^f$	$2^j\, C_{0j}^N$	$C_{0j}^{[1]}$	$C_{0j}^{[8]}$
0	−0.50000000000000	1.4631484256449	2.9908803661052	5.3672341813001
1	−1.4299560445655	1.1378636777296	1.5413614947768	2.6955279484399
2	1.9166666666667	−2.2500000000000	1.7184021483612	−1.6007519167030
3	0.61111111111111	−0.61959019752306	−2.0642440567933	−1.5427483775876
4	−0.64351851851852	0.19595791897636	−0.013041375932536	−0.30341867173287
5	0.34027777777778	−0.041373974809664	−0.23831132043848	−0.66995761696499
6	−0.32555555555556	0.050632425392143	−0.29505564506105	−0.76483272256170
7	0.22645502645503	−0.0085130103757183	−0.33982237796946	−0.89088866631223
8	−0.21839569160998	0.021364564886038	−0.39014664025160	−1.0512016932370
9	0.16922949735450	−0.0021163793679548	−0.46132229463197	−1.2231379052781
10	−0.16440329218107	0.011352248256237	−0.54181900555092	−1.4140169880252
11	0.13501683501684	−0.00031876770238782	−0.62865298103254	−1.6193130343325
12	−0.13184113865932	0.0069044046901382	−0.72327561055935	−1.8406888957442
13	0.11229279979280	0.00026524868288686	−0.82599364970112	−2.0771148764280
14	−0.11005447543909	0.0045886802251189	−0.93646341983044	−2.3289420592043
15	0.096110238967382	0.00045367535620384	−1.0545144536797	−2.5959150798748
16	−0.094451058201058	0.0032466294330511	−1.1801975461308	−2.8780968527867
17	0.084002246732026	0.00049759837275320	−1.3135046985544	−3.1754140946729
18	−0.082724593105216	0.0024063111971173	−1.4544109140733	−3.4878694626044
19	0.074602810584923	0.00048632461101711	−1.6028971675594	−3.8154359820062
20	−0.073589309531138	0.0018484695198520	−1.7589576701531	−4.1581059460687
21	0.067094820384294	0.00045472318488549	−1.9225846311898	−4.5158659968494
22	−0.066271559128702	0.0014608181493982	−2.0937708334094	−4.8887083360078
23	0.060959681513041	0.00041715324450384	−2.2725100912738	−5.2766246918423
24	−0.060277873250463	0.0011813528773489	−2.4587976549535	−5.6796088121000
25	0.055852455716586	0.00037961316951524	−2.6526292535445	−6.0976549233305
26	−0.055278632478632	0.00097371475344293	−2.8540011625229	−6.5307582257733
27	0.051534808970706	0.00034450885468517	−3.0629101297186	−6.9789144511760
28	−0.051045262465016	0.00081551052326244	−3.2793533396823	−7.4421199171304
29	0.047836791166019	0.00031265716431784	−3.5033283074846	−7.9203713698022
30	−0.047414264952909	0.00069237305414920	−3.7348328397738	−8.4136659536719
31	0.044633955423722	0.00028417060994145	−3.9738649934083	−8.9220011379835
32	−0.044265594288357	0.00059476050997821	−4.2204230432240	−9.4453746793249
33	0.041833086408439	0.00025886130696172	−4.4745054503731	−9.9837845786079
34	−0.041509119717676	0.00051614527601586	−4.7361108384675	−10.537229050602
35	0.039362982269557	0.00023642858405518	−5.0052379727688	−11.105706495350
36	−0.039075852563248	0.00045194571806451	−5.2818857426495	−11.689215475273
37	0.037168319112764	0.00021654582243161	−5.5660531463308	−12.287754694956
38	−0.036912089899288	0.00039887305714912	−5.8577392779563	−12.901322984173
39	0.035205459028174	0.00019889927248022	−6.1569433164241	−13.529919283126
40	−0.034975402839775	0.00035451933700361	−6.4636645157488	−14.173542629791

Table 10. Coefficients of the term including $\ln^0(1-z)$ in the asymptotic expansion at $z = 1$.

JHEP04(2019)116

References

[1] G.T. Bodwin, E. Braaten and G.P. Lepage, *Rigorous QCD analysis of inclusive annihilation and production of heavy quarkonium*, *Phys. Rev.* **D 51** (1995) 1125 [*Erratum ibid.* **D 55** (1997) 5853] [hep-ph/9407339] [INSPIRE].

[2] M. Krämer, *QCD corrections to inelastic J/ψ photoproduction*, *Nucl. Phys.* **B 459** (1996) 3 [hep-ph/9508409] [INSPIRE].

[3] M. Klasen, B.A. Kniehl, L.N. Mihaila and M. Steinhauser, *J/ψ plus jet associated production in two-photon collisions at next-to-leading order*, *Nucl. Phys.* **B 713** (2005) 487 [hep-ph/0407014] [INSPIRE].

[4] Y.-J. Zhang, Y.-j. Gao and K.-T. Chao, *Next-to-leading order QCD correction to $e^+e^- \to J/\psi + \eta_c$ at $\sqrt{s} = 10.6\,GeV$*, *Phys. Rev. Lett.* **96** (2006) 092001 [hep-ph/0506076] [INSPIRE].

[5] Y.-J. Zhang and K.-T. Chao, *Double-charm production $e^+e^- \to J/\psi + c\bar{c}$ at B factories with next-to-leading-order QCD corrections*, *Phys. Rev. Lett.* **98** (2007) 092003 [hep-ph/0611086] [INSPIRE].

[6] Y.-Q. Ma, Y.-J. Zhang and K.-T. Chao, *QCD corrections to $e^+e^- \to J/\psi + gg$ at B factories*, *Phys. Rev. Lett.* **102** (2009) 162002 [arXiv:0812.5106] [INSPIRE].

[7] B. Gong and J.-X. Wang, *Next-to-leading-order QCD corrections to $e^+e^- \to J/\psi gg$ at the B factories*, *Phys. Rev. Lett.* **102** (2009) 162003 [arXiv:0901.0117] [INSPIRE].

[8] Y.-J. Zhang, Y.-Q. Ma, K. Wang and K.-T. Chao, *QCD radiative correction to color-octet J/ψ inclusive production at B factories*, *Phys. Rev.* **D 81** (2010) 034015 [arXiv:0911.2166] [INSPIRE].

[9] J.M. Campbell, F. Maltoni and F. Tramontano, *QCD corrections to J/ψ and Υ production at hadron colliders*, *Phys. Rev. Lett.* **98** (2007) 252002 [hep-ph/0703113] [INSPIRE].

[10] B. Gong, X.Q. Li and J.-X. Wang, *QCD corrections to J/ψ production via color octet states at Tevatron and LHC*, *Phys. Lett.* **B 673** (2009) 197 [*Erratum ibid.* **B 693** (2010) 612] [arXiv:0805.4751] [INSPIRE].

[11] M. Butenschön and B.A. Kniehl, *Complete next-to-leading-order corrections to J/ψ photoproduction in nonrelativistic quantum chromodynamics*, *Phys. Rev. Lett.* **104** (2010) 072001 [arXiv:0909.2798] [INSPIRE].

[12] Y.-Q. Ma, K. Wang and K.-T. Chao, *QCD radiative corrections to χ_{cJ} production at hadron colliders*, *Phys. Rev.* **D 83** (2011) 111503 [arXiv:1002.3987] [INSPIRE].

[13] Y.-Q. Ma, K. Wang and K.-T. Chao, *$J/\psi(\psi')$ production at the Tevatron and LHC at $\mathcal{O}(\alpha_s^4 v^4)$ in nonrelativistic QCD*, *Phys. Rev. Lett.* **106** (2011) 042002 [arXiv:1009.3655] [INSPIRE].

[14] M. Butenschön and B.A. Kniehl, *Reconciling J/ψ production at HERA, RHIC, Tevatron, and LHC with nonrelativistic QCD factorization at next-to-leading order*, *Phys. Rev. Lett.* **106** (2011) 022003 [arXiv:1009.5662] [INSPIRE].

JHEP04(2019)116

[15] M. Butenschön and B.A. Kniehl, *Probing nonrelativistic QCD factorization in polarized J/ψ photoproduction at next-to-leading order*, *Phys. Rev. Lett.* **107** (2011) 232001 [arXiv:1109.1476] [INSPIRE].

[16] M. Butenschön and B.A. Kniehl, *J/ψ polarization at the Tevatron and the LHC: nonrelativistic-QCD factorization at the crossroads*, *Phys. Rev. Lett.* **108** (2012) 172002 [arXiv:1201.1872] [INSPIRE].

[17] K.-T. Chao, Y.-Q. Ma, H.-S. Shao, K. Wang and Y.-J. Zhang, *J/ψ polarization at hadron colliders in nonrelativistic QCD*, *Phys. Rev. Lett.* **108** (2012) 242004 [arXiv:1201.2675] [INSPIRE].

[18] B. Gong, L.-P. Wan, J.-X. Wang and H.-F. Zhang, *Polarization for prompt J/ψ and $\psi(2s)$ production at the Tevatron and LHC*, *Phys. Rev. Lett.* **110** (2013) 042002 [arXiv:1205.6682] [INSPIRE].

[19] K. Wang, Y.-Q. Ma and K.-T. Chao, *$\Upsilon(1S)$ prompt production at the Tevatron and LHC in nonrelativistic QCD*, *Phys. Rev.* **D 85** (2012) 114003 [arXiv:1202.6012] [INSPIRE].

[20] B. Gong, L.-P. Wan, J.-X. Wang and H.-F. Zhang, *Complete next-to-leading-order study on the yield and polarization of $\Upsilon(1S, 2S, 3S)$ at the Tevatron and LHC*, *Phys. Rev. Lett.* **112** (2014) 032001 [arXiv:1305.0748] [INSPIRE].

[21] H. Han et al., *$\Upsilon(nS)$ and $\chi_b(nP)$ production at hadron colliders in nonrelativistic QCD*, *Phys. Rev.* **D 94** (2016) 014028 [arXiv:1410.8537] [INSPIRE].

[22] M. Butenschön, Z.-G. He and B.A. Kniehl, *η_c production at the LHC challenges nonrelativistic QCD factorization*, *Phys. Rev. Lett.* **114** (2015) 092004 [arXiv:1411.5287] [INSPIRE].

[23] H. Han, Y.-Q. Ma, C. Meng, H.-S. Shao and K.-T. Chao, *η_c production at LHC and indications on the understanding of J/ψ production*, *Phys. Rev. Lett.* **114** (2015) 092005 [arXiv:1411.7350] [INSPIRE].

[24] H.-F. Zhang, Z. Sun, W.-L. Sang and R. Li, *Impact of η_c hadroproduction data on charmonium production and polarization within nonrelativistic QCD framework*, *Phys. Rev. Lett.* **114** (2015) 092006 [arXiv:1412.0508] [INSPIRE].

[25] G.T. Bodwin et al., *Fragmentation contributions to hadroproduction of prompt J/ψ, χ_{cJ}, and $\psi(2S)$ states*, *Phys. Rev.* **D 93** (2016) 034041 [arXiv:1509.07904] [INSPIRE].

[26] Y.-Q. Ma and K.-T. Chao, *A new factorization theory for heavy quarkonium production and decay*, arXiv:1703.08402 [INSPIRE].

[27] J.C. Collins, D.E. Soper and G.F. Sterman, *Factorization of hard processes in QCD*, *Adv. Ser. Direct. High Energy Phys.* **5** (1989) 1 [hep-ph/0409313] [INSPIRE].

[28] Z.-B. Kang, J.-W. Qiu and G. Sterman, *Heavy quarkonium production and polarization*, *Phys. Rev. Lett.* **108** (2012) 102002 [arXiv:1109.1520] [INSPIRE].

[29] Z.-B. Kang, Y.-Q. Ma, J.-W. Qiu and G. Sterman, *Heavy quarkonium production at collider energies: factorization and evolution*, *Phys. Rev.* **D 90** (2014) 034006 [arXiv:1401.0923] [INSPIRE].

[30] Z.-B. Kang, Y.-Q. Ma, J.-W. Qiu and G. Sterman, *Heavy quarkonium production at collider energies: partonic cross section and polarization*, *Phys. Rev.* **D 91** (2015) 014030 [arXiv:1411.2456] [INSPIRE].

JHEP04(2019)116

[31] S. Fleming, A.K. Leibovich, T. Mehen and I.Z. Rothstein, *The systematics of quarkonium production at the LHC and double parton fragmentation*, *Phys. Rev.* **D 86** (2012) 094012 [arXiv:1207.2578] [INSPIRE].

[32] S. Fleming, A.K. Leibovich, T. Mehen and I.Z. Rothstein, *Anomalous dimensions of the double parton fragmentation functions*, *Phys. Rev.* **D 87** (2013) 074022 [arXiv:1301.3822] [INSPIRE].

[33] V.N. Gribov and L.N. Lipatov, *Deep inelastic ep scattering in perturbation theory*, *Sov. J. Nucl. Phys.* **15** (1972) 438 [*Yad. Fiz.* **15** (1972) 781] [INSPIRE].

[34] G. Altarelli and G. Parisi, *Asymptotic freedom in parton language*, *Nucl. Phys.* **B 126** (1977) 298 [INSPIRE].

[35] Y.L. Dokshitzer, *Calculation of the structure functions for deep inelastic scattering and e^+e^- annihilation by perturbation theory in quantum chromodynamics*, *Sov. Phys. JETP* **46** (1977) 641 [*Zh. Eksp. Teor. Fiz.* **73** (1977) 1216] [INSPIRE].

[36] E. Braaten, K.-m. Cheung and T.C. Yuan, *Z^0 decay into charmonium via charm quark fragmentation*, *Phys. Rev.* **D 48** (1993) 4230 [hep-ph/9302307] [INSPIRE].

[37] E. Braaten and T.C. Yuan, *Gluon fragmentation into heavy quarkonium*, *Phys. Rev. Lett.* **71** (1993) 1673 [hep-ph/9303205] [INSPIRE].

[38] P.L. Cho, M.B. Wise and S.P. Trivedi, *Gluon fragmentation into polarized charmonium*, *Phys. Rev.* **D 51** (1995) R2039 [hep-ph/9408352] [INSPIRE].

[39] E. Braaten and T.C. Yuan, *Gluon fragmentation into P-wave heavy quarkonium*, *Phys. Rev.* **D 50** (1994) 3176 [hep-ph/9403401] [INSPIRE].

[40] M. Beneke and I.Z. Rothstein, *ψ' polarization as a test of colour octet quarkonium production*, *Phys. Lett.* **B 372** (1996) 157 [*Erratum ibid.* **B 389** (1996) 769] [hep-ph/9509375] [INSPIRE].

[41] J.P. Ma, *Quark fragmentation into ${}^3P_J$ quarkonium*, *Phys. Rev.* **D 53** (1996) 1185 [hep-ph/9504263] [INSPIRE].

[42] E. Braaten and Y.-Q. Chen, *Dimensional regularization in quarkonium calculations*, *Phys. Rev.* **D 55** (1997) 2693 [hep-ph/9610401] [INSPIRE].

[43] E. Braaten and J. Lee, *Next-to-leading order calculation of the color-octet ${}^3S_1$ gluon fragmentation function for heavy quarkonium*, *Nucl. Phys.* **B 586** (2000) 427 [hep-ph/0004228] [INSPIRE].

[44] G. Hao, Y. Zuo and C.-F. Qiao, *The fragmentation function of gluon splitting into P-wave spin-singlet heavy quarkonium*, arXiv:0911.5539 [INSPIRE].

[45] Y. Jia, W.-L. Sang and J. Xu, *Inclusive h_c production at B factories*, *Phys. Rev.* **D 86** (2012) 074023 [arXiv:1206.5785] [INSPIRE].

[46] G.T. Bodwin, H.S. Chung, U.-R. Kim and J. Lee, *Quark fragmentation into spin-triplet S-wave quarkonium*, *Phys. Rev.* **D 91** (2015) 074013 [arXiv:1412.7106] [INSPIRE].

[47] Y.-Q. Ma, J.-W. Qiu and H. Zhang, *Heavy quarkonium fragmentation functions from a heavy quark pair. I. S wave*, *Phys. Rev.* **D 89** (2014) 094029 [arXiv:1311.7078] [INSPIRE].

[48] Y.-Q. Ma, J.-W. Qiu and H. Zhang, *Fragmentation functions of polarized heavy quarkonium*, *JHEP* **06** (2015) 021 [arXiv:1501.04556] [INSPIRE].

JHEP04(2019)116

[49] E. Braaten and T.C. Yuan, *Gluon fragmentation into spin-triplet S-wave quarkonium*, *Phys. Rev.* **D 52** (1995) 6627 [hep-ph/9507398] [INSPIRE].

[50] G.T. Bodwin and J. Lee, *Relativistic corrections to gluon fragmentation into spin-triplet S-wave quarkonium*, *Phys. Rev.* **D 69** (2004) 054003 [hep-ph/0308016] [INSPIRE].

[51] G.T. Bodwin, U.-R. Kim and J. Lee, *Higher-order relativistic corrections to gluon fragmentation into spin-triplet S-wave quarkonium*, *JHEP* **11** (2012) 020 [arXiv:1208.5301] [INSPIRE].

[52] P. Zhang, Y.-Q. Ma, Q. Chen and K.-T. Chao, *Analytical calculation for the gluon fragmentation into spin-triplet S-wave quarkonium*, *Phys. Rev.* **D 96** (2017) 094016 [arXiv:1708.01129] [INSPIRE].

[53] Q.-F. Sun, Y. Jia, X. Liu and R. Zhu, *Inclusive h_c production and energy spectrum from e^+e^- annihilation at a super B factory*, *Phys. Rev.* **D 98** (2018) 014039 [arXiv:1801.10137] [INSPIRE].

[54] P. Artoisenet and E. Braaten, *Gluon fragmentation into quarkonium at next-to-leading order*, *JHEP* **04** (2015) 121 [arXiv:1412.3834] [INSPIRE].

[55] LHCb collaboration, *Measurement of the $\eta_c(1S)$ production cross-section in proton-proton collisions via the decay $\eta_c(1S) \to p\bar{p}$*, *Eur. Phys. J.* **C 75** (2015) 311 [arXiv:1409.3612] [INSPIRE].

[56] G.T. Bodwin, H.S. Chung, U.-R. Kim and J. Lee, *Fragmentation contributions to J/ψ production at the Tevatron and the LHC*, *Phys. Rev. Lett.* **113** (2014) 022001 [arXiv:1403.3612] [INSPIRE].

[57] P. Faccioli, V. Knünz, C. Lourenço, J. Seixas and H.K. Wöhri, *Quarkonium production in the LHC era: a polarized perspective*, *Phys. Lett.* **B 736** (2014) 98 [arXiv:1403.3970] [INSPIRE].

[58] K.G. Chetyrkin and F.V. Tkachov, *Integration by parts: the algorithm to calculate β-functions in 4 loops*, *Nucl. Phys.* **B 192** (1981) 159 [INSPIRE].

[59] S. Laporta, *High precision calculation of multiloop Feynman integrals by difference equations*, *Int. J. Mod. Phys.* **A 15** (2000) 5087 [hep-ph/0102033] [INSPIRE].

[60] C. Studerus, *Reduze-Feynman integral reduction in C++*, *Comput. Phys. Commun.* **181** (2010) 1293 [arXiv:0912.2546] [INSPIRE].

[61] R.N. Lee, *Presenting LiteRed: a tool for the Loop InTEgrals REDuction*, arXiv:1212.2685 [INSPIRE].

[62] A.V. Smirnov, *FIRE5: a C++ implementation of Feynman Integral REduction*, *Comput. Phys. Commun.* **189** (2015) 182 [arXiv:1408.2372] [INSPIRE].

[63] J.C. Collins and D.E. Soper, *Parton distribution and decay functions*, *Nucl. Phys.* **B 194** (1982) 445 [INSPIRE].

[64] A.V. Kotikov, *Differential equations method: new technique for massive Feynman diagrams calculation*, *Phys. Lett.* **B 254** (1991) 158 [INSPIRE].

[65] Z. Bern, L.J. Dixon and D.A. Kosower, *Dimensionally regulated one loop integrals*, *Phys. Lett.* **B 302** (1993) 299 [*Erratum ibid.* **B 318** (1993) 649] [hep-ph/9212308] [INSPIRE].

[66] E. Remiddi, *Differential equations for Feynman graph amplitudes*, *Nuovo Cim.* **A 110** (1997) 1435 [hep-th/9711188] [INSPIRE].

JHEP04(2019)116

[67] T. Gehrmann and E. Remiddi, *Differential equations for two loop four point functions*, *Nucl. Phys.* **B 580** (2000) 485 [hep-ph/9912329] [INSPIRE].

[68] J.M. Henn, *Multiloop integrals in dimensional regularization made simple*, *Phys. Rev. Lett.* **110** (2013) 251601 [arXiv:1304.1806] [INSPIRE].

[69] R.N. Lee, *Reducing differential equations for multiloop master integrals*, *JHEP* **04** (2015) 108 [arXiv:1411.0911] [INSPIRE].

[70] L. Adams, E. Chaubey and S. Weinzierl, *Simplifying differential equations for multiscale Feynman integrals beyond multiple polylogarithms*, *Phys. Rev. Lett.* **118** (2017) 141602 [arXiv:1702.04279] [INSPIRE].

[71] M. Caffo, H. Czyż, M. Gunia and E. Remiddi, *BOKASUN: a fast and precise numerical program to calculate the master integrals of the two-loop sunrise diagrams*, *Comput. Phys. Commun.* **180** (2009) 427 [arXiv:0807.1959] [INSPIRE].

[72] M. Czakon, *Tops from light quarks: full mass dependence at two-loops in QCD*, *Phys. Lett.* **B 664** (2008) 307 [arXiv:0803.1400] [INSPIRE].

[73] R. Mueller and D.G. Öztürk, *On the computation of finite bottom-quark mass effects in Higgs boson production*, *JHEP* **08** (2016) 055 [arXiv:1512.08570] [INSPIRE].

[74] R.N. Lee, A.V. Smirnov and V.A. Smirnov, *Solving differential equations for Feynman integrals by expansions near singular points*, *JHEP* **03** (2018) 008 [arXiv:1709.07525] [INSPIRE].

[75] X. Liu, Y.-Q. Ma and C.-Y. Wang, *A systematic and efficient method to compute multi-loop master integrals*, *Phys. Lett.* **B 779** (2018) 353 [arXiv:1711.09572] [INSPIRE].

[76] X. Liu and Y.-Q. Ma, *Determine arbitrary Feynman integrals by vacuum integrals*, arXiv:1801.10523 [INSPIRE].

[77] A.B. Goncharov, *Multiple polylogarithms and mixed Tate motives*, math.AG/0103059 [INSPIRE].

[78] H. Frellesvig, D. Tommasini and C. Wever, *On the reduction of generalized polylogarithms to Li_n and $Li_{2,2}$ and on the evaluation thereof*, *JHEP* **03** (2016) 189 [arXiv:1601.02649] [INSPIRE].

[79] J.M. Henn, *Lectures on differential equations for Feynman integrals*, *J. Phys.* **A 48** (2015) 153001 [arXiv:1412.2296] [INSPIRE].

[80] T. Binoth and G. Heinrich, *An automatized algorithm to compute infrared divergent multiloop integrals*, *Nucl. Phys.* **B 585** (2000) 741 [hep-ph/0004013] [INSPIRE].

[81] G. Heinrich, *Sector decomposition*, *Int. J. Mod. Phys.* **A 23** (2008) 1457 [arXiv:0803.4177] [INSPIRE].

[82] J. Carter and G. Heinrich, *SecDec: a general program for sector decomposition*, *Comput. Phys. Commun.* **182** (2011) 1566 [arXiv:1011.5493] [INSPIRE].

[83] S. Borowka, J. Carter and G. Heinrich, *SecDec: a tool for numerical multi-loop calculations*, *J. Phys. Conf. Ser.* **368** (2012) 012051 [arXiv:1206.4908] [INSPIRE].

[84] S. Borowka, J. Carter and G. Heinrich, *Numerical evaluation of multi-loop integrals for arbitrary kinematics with SecDec 2.0*, *Comput. Phys. Commun.* **184** (2013) 396 [arXiv:1204.4152] [INSPIRE].

JHEP04(2019)116

[85] S. Borowka and G. Heinrich, *Massive non-planar two-loop four-point integrals with SecDec 2.1*, *Comput. Phys. Commun.* **184** (2013) 2552 [arXiv:1303.1157] [INSPIRE].

[86] A.V. Smirnov and M.N. Tentyukov, *Feynman Integral Evaluation by a Sector decomposiTion Approach (FIESTA)*, *Comput. Phys. Commun.* **180** (2009) 735 [arXiv:0807.4129] [INSPIRE].

[87] A.V. Smirnov, V.A. Smirnov and M. Tentyukov, *FIESTA 2: parallelizeable multiloop numerical calculations*, *Comput. Phys. Commun.* **182** (2011) 790 [arXiv:0912.0158] [INSPIRE].

[88] A.V. Smirnov, *FIESTA 3: cluster-parallelizable multiloop numerical calculations in physical regions*, *Comput. Phys. Commun.* **185** (2014) 2090 [arXiv:1312.3186] [INSPIRE].

[89] A.V. Smirnov, *FIESTA4: optimized Feynman integral calculations with GPU support*, *Comput. Phys. Commun.* **204** (2016) 189 [arXiv:1511.03614] [INSPIRE].

[90] P. Artoisenet and E. Braaten, *Gluon fragmentation into quarkonium at next-to-leading order using FKS subtraction*, *JHEP* **01** (2019) 227 [arXiv:1810.02448] [INSPIRE].

[91] F. Feng and Y. Jia, *Next-to-leading-order QCD corrections to gluon fragmentation into* ${}^1S_0^{(1,8)}$ *quarkonia*, arXiv:1810.04138 [INSPIRE].

JHEP04(2019)116